Exploring the impact of chloride-induced corrosion on seismic damage limit states and residual capacity of RC structures

Ebrahim Afsar Dizaj[a], Rahmat Madandoust[b] and Mohammad M Kashani[c]*

[a] *PhD Candidate of Structural Engineering, University of Guilan, Faculty of Engineering, Rasht, Iran*

[b] *Associate professor, University of Guilan, Faculty of Engineering, Rasht, Iran*

[c] *Lecturer, University of Southampton (formerly University of Bristol), Faculty of Engineering, University of Southampton, Southampton, SO17 1BJ, UK (corresponding author), Email: mehdi.kashani@soton.ac.uk*

Exploring the impact of chloride-induced corrosion on seismic damage limit states and residual capacity of RC structures

Abstract

A nonlinear finite element (FE) framework for time-dependent capacity assessment of corroded rectangular RC columns is developed. The proposed nonlinear FE model includes the impact of corrosion on inelastic buckling and low-cycle fatigue degradation of longitudinal reinforcement. The proposed nonlinear FE model is validated against a set of experimental data and then extended to evaluate the impact of corrosion on damage limit states to be used in seismic performance and evaluation of corroded structures. This is done through a parametric study on hypothetical RC columns, varied in axial force ratios, mass loss ratios, cover crack widths, and confinement levels. Moreover, the application of the proposed model in seismic collapse capacity assessment of corroded structures is shown through nonlinear dynamic analyses of prototype columns. Results show that, depending on the axial force ratio, corrosion changes the failure mechanism of the columns. The results of this study suggest for seismic fragility analysis of corroded structures the damage limit states should be considered as time-variant parameters.

Nomenclature

T_{corr} time to corrosion initiation of steel bar

C_0 initial chloride content

$C_{S,\Delta x}$ chloride content at depth Δx and time t

C_{crit} critical chloride concentration

X depth of concrete cover

Δx depth of the convection zone

$D_{app,C}$ apparent coefficient of chloride diffusion

erf(z) error function

K_e environmental transfer variable

b_e regression variable

T_{ref} standard test temperature

T_{real} temperature of the structural element or the ambient air

P_{ave} average corrosion penetration depth based on the uniform volumetric mass loss

$P_{ave}(t)$ average corrosion penetration depth based on the uniform volumetric mass loss at time t after corrosion initiation

$A(t)$ ageing parameter

a ageing exponent

t_0 reference point of time

$DRCM,0$ chloride migration coefficient

$\psi(t)$ percentage of mass loss of vertical reinforcements

$\psi_{tie}(t)$ percentage of mass loss of ties

$D(t)$ residual bar diameter

D_0 initial bar diameter

α pitting coefficient

$i_{corr}(t)$ time-dependent corrosion current density

i_{corr0} corrosion current density at corrosion initiation time T_{corr}

t_{cr} time to crack initiation

W_{crit} total amount of critical rust products

k_p rate of the production of corrosion products

w crack width

ΔA_s steel loss of the reinforcing bar cross section

ΔA_{s0} steel cross section loss needed for crack initiation

w_{lim} crack width limit

Δp_{lim} additional corrosion penetration corresponding to the limit crack width

p_0 corrosion penetration corresponding to ΔA_{s0}

t_f time of failure

σ_c compressive strength of concrete

σ_{yh} yield strength of steel hoops

$\sigma_{yh}(t)$ yield strength of hoops at time t after corrosion initiation

$\varepsilon_{cu}(t)$ ultimate strain of confined concrete at time t after corrosion initiation

$\varepsilon_{uh}(t)$ transverse steel strain at maximum steel stress at time t after corrosion initiation

ε_{uh} transverse steel strain at maximum steel stress

σ_{cc} (t) compressive strength of confined concrete at time t after corrosion initiation

K_c confined concrete increase factor

ρ_s volumetric ratio of the rectangular steel hoops

ρ_s (t) volumetric ratio of the rectangular steel hoops at time t after corrosion initiation

P_0 perimeter of the uncorroded column section

P_{corr} perimeter of the corroded column section

n_{bars} number of bars in column section

w_{cr} total crack width for a given corrosion level

v_{rust} ratio of the volumetric expansion of the corrosion products with respect to the uncorroded steel

E_{force} normalized hysteretic force error

E_{energy} normalized hysteretic energy error

F_{calc} calculated lateral force at corresponding peak displacements

F_{meas} measured lateral force at corresponding peak displacements

Ω_{meas} measured area within the hysteresis loops

Ω_{calc} calculated area within the hysteresis loops

κ conversion factor from $\mu A/cm^2$ to mm/year

E_R normalized capacity

E_μ normalized ductility factor

R_{loss} capacity loss = (maximum lateral force of uncorroded column-maximum lateral force of corroded column) / maximum lateral force of uncorroded column

μ_{loss} ductility loss = (ductility factor of uncorroded column- ductility factor of corroded column) / ductility factor of uncorroded column

1. Introduction

Chloride induced corrosion of steel reinforcement in reinforced concrete (RC) bridges and structures, is one of the most important engineering and economic challenges in developed countries. Annually, corrosion of RC structures causes great cost for stakeholders and decision makers around the world (Chiu et al., 2015; Rao et al., 2016a). Moreover, there is a large number of existing RC structures in high seismicity regions around the world that are constructed prior to modern seismic design codes, and suffer from material ageing (ASCE, 2013).

At material scale, corrosion changes mechanical characteristics and ductility of reinforcing bars, reduces compressive strength of concrete cover due to cracking, and weaken the bond strength at the interface of concrete and reinforcement (Vu et al., 2016). In recent years, several studies have been conducted by other researchers to investigate the effects of corrosion on structural performance of RC components experimentally (Guo et al., 2015a;Meda et al., 2014; Ou et al., 2012). Almost all of these earlier studies have confirmed that corrosion affects the structural performance of the RC components significantly (i.e. reducing the flexural capacity and ductility). For instance, Meda et al. (2014) reported that the maximum strength and ultimate displacement capacity of a column with about 20% mass loss are reduced by 26% and 50 % respectively, in comparison to pristine column.

Furthermore, conventional seismic design of RC structures does not account for material ageing and time-dependent capacity of RC structures. However, corrosion results in damage in concrete (cover and core confined concrete) and embedded reinforcing bars. The simultaneous effects of seismic loads and progressive material ageing can lead to undesirable failure mechanisms, and considerably affects structural performance under dynamic earthquake loading (Camnasio, 2013; Titi, 2012). Therefore, to simulate the nonlinear behaviour and predict the time-dependent damage limit states (these are extremely important

in seismic vulnerability analysis) of corroded RC structures under seismic loading, it is necessary to consider the effects of material degradation due to corrosion. Therefore, there is an urgent need for development of a framework to effectively model the time-dependent capacity of existing corroded RC structures.

In previous studies (Alipour et al., 2010; Berto et al., 2009), several numerical models have been proposed to consider the corrosion of reinforcements. All of these models are simple models based on average reduced cross-sectional area of corroded reinforcing bars and the impact of corrosion on inelastic buckling and low-cycle fatigue degradation are not considered. However, experimental and computational studies on reinforcing bars conducted by Kashani et al. (2013a, 2013b,2015) and Fernandez et al.(2015, 2016), and experimental testing of corroded RC columns conducted by Ma et al. (2012) and Li et al.(2015) shows that the impact of the corrosion damage on inelastic buckling and low-cycle fatigue degradation of reinforcing bars is significant. Furthermore, other researchers attempted to develop fragility curves for corroded bridges and structures (Ghosh & Padgett, 2010; Ni Choine et al., 2016; Rao et al., 2016b). However, in all of these studies, the damage limit states used in development of fragility curves for corroded RC structures were those suggested for uncorroded RC structures (FEMA, 1999). This is due to the significant paucity in the literature to provide a quantitative methodology/technique to evaluate the damage limit states for corroded RC components/structures.

Accordingly, in this study, a nonlinear finite element (FE) framework for time-dependent capacity assessment of corroded rectangular RC columns is developed. The framework consists of two parts. The first part uses a set of analytical models, available in the literature, to simulate the corrosion initiation time, corrosion induced cover crack initiation time, and time-dependent crack propagation. The second part develops an advanced nonlinear FE model to predict the time-dependent residual capacity of corroded RC structures. The

proposed framework in this paper, relates the mass loss, as a measure of corrosion damage, and corresponding cover crack width of corroded RC components at time *t*, to its residual collapse capacity at time *t*. The proposed framework significantly improves the prior models, as it is able to relate the observed visual damage (e.g. measured crack width in visual inspection of an RC structure in the real world) to the residual capacity of the structure at the time of inspection. The proposed nonlinear FE model is validated against a set of experimental data reported in (Meda et al., 2014). Following the validation of the FE model, a parametric study is conducted for two types of prototype RC column details (low confined and well confined) to evaluate and quantify the impact of corrosion on damage limit states. The evaluation of the time-dependent damage limit states for corroded RC columns/components is another major advancement that this paper will make to the earlier models. The result of parametric study shows that corrosion has a more significant impact on ductility loss (μ_{loss}) of corroded RC columns than flexural capacity. For example, the analyses results show that 15% mass loss corresponds to 1.5 mm crack width in concrete cover, which results in approximately 25%-45% flexural capacity and 45-60% ductility loss of corroded columns, depending on the axial force ratio. Finally, through incremental dynamic analyses, the application of the proposed model in seismic collapse capacity assessment of corroded structures is shown.

2. Overview of the framework for residual capacity assessment of corroded RC structures

The main objectives of the study is to develop a FE framework (Fig. 1) to model the time-dependent nonlinear behaviour of corroded RC components/structures, and to predict their critical damage limits states for seismic vulnerability analysis. To this end, OpenSees (McKenna, 2011), a fibre-based FE code is employed. Fig .1 shows that the framework consists of two main parts. In part A, firstly nonlinear FE model of pristine and corroded

columns are developed and validated against experimental data available in the literature (Meda et al., 2014). To account for the impact of corrosion on nonlinear behaviour of corroded RC columns, the constitutive material models are modified. The methodology that is used to modify the material models is discussed in detail in section 3 of this paper. The details of model validation against experimental data are also available in section 3 of this paper.

In part B of the framework, the proposed FE model of the corroded column is employed in development of 3D time-dependent capacity surfaces and damage limit states of corroded columns. To this end, after evaluation of exposure time and corrosion initiation time (T_{corr}), at each time step, the material models are updated using percentage of mass loss at time t, and then a nonlinear pushover analysis is performed. In section 4, the time-dependent analyses and corrosion effects on critical damage limit states (flexural capacity, ductility and failure modes) are discussed.

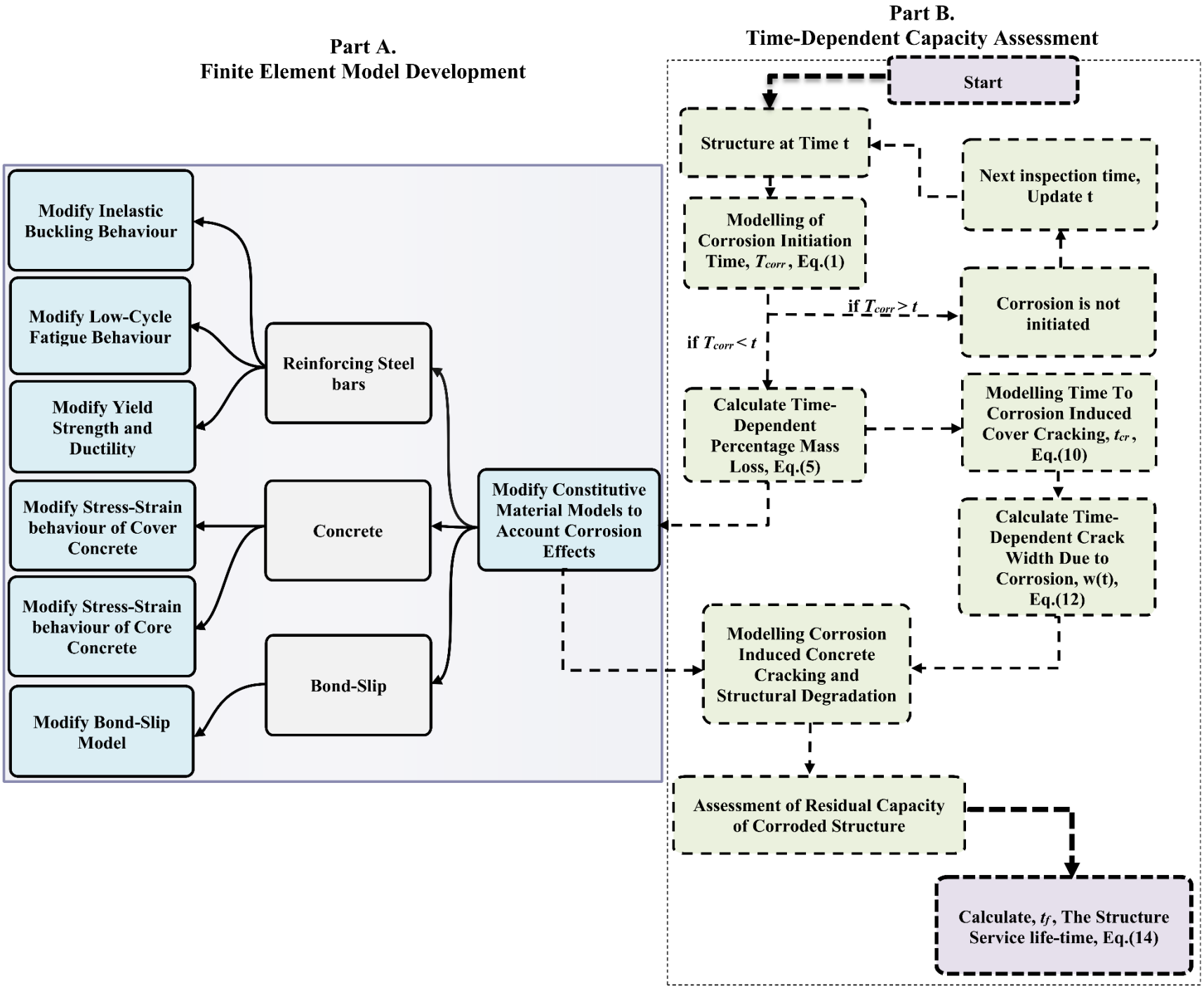

Fig. 1. The framework for residual capacity assessment of corroded RC structures

2.1 Modelling time to corrosion initiation

Structures located in marine environments, or structures exposed to de-icing salts in winter from adjacent roads, are vulnerable to chloride induced corrosion (Kashani, 2014). Chloride ions can also be presented in buildings for particular industrial applications (Broomfield, 2002). Corrosion starts when the chloride content at reinforcement level reaches a critical threshold, which depends on several parameters including electrochemical potential of the reinforcement, the presence of oxygen, and the conditions of saturation (Camnasio, 2013). There are several models available in the literature for predicting the corrosion initiation time due to chloride ions (Guo et al., 2015b;Shafei et al., 2012; Zhang et al., 2015). Shafei et al., (2012) estimated the diffusion coefficient considering the influence of ambient temperature, relative humidity, carbonation process, concrete age and free chloride content. Other than mentioned method, Zhang et al.(2015) considered the existence of initial defects occurring in the formation of concrete mixture as another influence factor that affecting the whole corrosion process. The *fib* model code (fib, 2006) proposes in particular, a full probabilistic design approach for modelling of chloride induced corrosion service life of RC structures. Since most observations indicate that the transport of chlorides in concrete is diffusion controlled (Tang et al., 2015), in all of these models the rate of chloride ingress is modelled using the Fick's 2nd law of diffusion (Poulsen & Mejlbro, 2010).

The time to corrosion initiation of embedded reinforcing bars inside concrete, T_{corr}, can be evaluated using the Eq. (1) (fib, 2006):

$$T_{corr} = \frac{(X - \Delta x)^2}{4D_{app,C}} \left[1 - \mathrm{erf}^{-1}\left(\frac{C_{s,\Delta x} - C_{crit}}{C_{s,\Delta x} - C_0}\right) \right]^{-2} \quad (1)$$

where $D_{app,C}$ is the apparent coefficient of chloride diffusion, C_{crit} is the critical chloride concentration, C_0 is the initial chloride content in the cement paste, X is the depth of concrete

cover, Δx is the depth of the convection zone, $C_{S,\Delta x}$ is the chloride content at depth Δx, and erf(z) is the error function.

In this study, the procedure outlined in *fib* (fib, 2006) is used for calculation of the apparent diffusion coefficient (Eq. (2)).

$$D_{app,C} = k_e D_{RCM,0} k_t A(t) \tag{2}$$

where, K_e is the environmental transfer variable as described in Eq.(3):

$$K_e = \exp\left[b_e \left(\frac{1}{T_{ref}} - \frac{1}{T_{real}}\right)\right] \tag{3}$$

b_e is the regression variable with mean and standard deviation values of 4800K and 700K respectively, T_{ref} is the standard test temperature that can be taken as 293K, T_{real} is the temperature of the structural element or the ambient air that can be determined using the available data from the nearest weather station, K_t is the transfer variable equal to 1 and $A(t)$ is the ageing parameter as described in Eq. (4):

$$A(t) = \left(\frac{t_0}{t}\right)^a \tag{4}$$

where, a is the ageing exponent to be taken as 0.3 and t_0 is the reference point of time that can be taken as 0.0767 years (t_0 = 28 days). The fib (2006) recommended values of mean and standard deviation for the parameters involved in the diffusion process are tabulated in Table 1.

Table 1. Parameters of the random variables involved in the diffusion process

Random Variable	Distribution type	μ	σ
X (*mm*)	Normal	40	8
a	Beta	0.3	0.12
Δx (mm)	Constant	0	-
$C_{S,\Delta x}$	Normal	3	0.3 μ
$D_{RCM,0}$ (m^2/s)	Normal	15.8×10^{-12}	0.2 μ
C_{crit}	Beta	0.6	0.15
C_0	Uniform	0	-

Once T_{corr} is estimated, the time-dependent percentage of mass loss of the corroded reinforcement at time *t* after corrosion initiation, $\psi(t)$, can be evaluated using Eq. (5).

$$\psi(t) = \left[1 - \left(\frac{D(t)}{D_0}\right)^2\right] \times 100 \quad (5)$$

$$D(t) = D_0 - \alpha P_{ave}(t) \quad (6)$$

where $D(t)$ is the residual bar diameter at time *t* after corrosion initiation, D_0 is the initial bar diameter, and α is the ratio of the maximum pitting depth to the average reduced area known as the pitting coefficient. The value of α is 2 for uniform corrosion and varied from 4 to 8 for pitting corrosion (Vidal et al., 2004). The $P_{ave}(t)$ is average corrosion penetration depth based on the uniform volumetric mass loss at time *t* after corrosion initiation which can be calculated as follows:

$$P_{ave}(t) = \kappa \int_{T_{cor}}^{t} i_{corr}(t)\, dt \quad (7)$$

where, $i_{corr}(t)$ is the corrosion current density at time *t* after corrosion initiation in $\mu A/cm^2$ and $\kappa=0.0116$ is the conversion factor from $\mu A/cm^2$ to mm/year. The time dependent corrosion current density can be estimated using Eqs. (8-9) (Vu & Stewart, 2000):

$$i_{corr}(t) = 0.85\, i_{corr\,0}(t - T_{corr})^{-0.29} \quad (8)$$

$$i_{corr\,0} = \frac{37.8(1 - w/c)^{-1.64}}{X} \quad (9)$$

where, i_{corr0} is the corrosion current density at corrosion initiation time T_{corr}, w/c is the water cement ratio of concrete and X is the thickness of concrete cover.

2.2 Modelling time to corrosion induced cover cracking

Once the concentrated chloride ions break down the passive film around the reinforcement, corrosion starts in the presence of moisture and oxygen. This process, results in formation of expansive corrosion products (rust) around the reinforcement. The volume of corrosion products is about four to six times larger than that of normal steel (Liu, 1996). This volume increase induces internal tensile stresses in the concrete cover, and when these stresses exceed the tensile strength of the concrete, the concrete cover is damaged by cracking, delamination and spalling. Different models have been proposed to predict the time to crack initiation, which can be divided into the four main groups such as (*i*) empirical models (Aligizaki, 1999;Webster & Clark, 2000), (*ii*) analytical models (Chernin et al., 2010; El Maaddawy & Soudki, 2007;), (*iii*) numerical models (Chernin & Val, 2011;Thoft-Christensen, 2005) and (*iv*) fracture mechanics based models (Williamson & Clark, 2000). In this research, the time to corrosion induced crack is modelled by a thick-wall cylinder model developed by Liu and Weyers (1998). This model considers that the corrosion products at initial cracking of the concrete will occupy three volumes. This includes the porous zone, the expansion of the concrete due to rust pressure, and the space of the corroded steel. Further details of the Liu and Weyers model are available in (Liu & Weyers, 1998). Using this model, the time to crack initiation is defined in Eq. (10):

$$t_{cr} = \frac{W_{crit}^{2}}{2k_{p}} \tag{10}$$

where, W_{crit} is the corresponding total amount of critical rust products to fill the mentioned volumes, k_p is the rate of the production of corrosion products given by the empirical Eq. (11)

suggested by Val (2007):

$$k_p = 9.8\times10^{-5}\,\frac{\pi D_0\, i_{corr}(t)}{0.57} \tag{11}$$

Further details and derivation of Eqs. (10) and (11) are available in (Val, 2007).

2.3 Modelling corrosion induced crack propagation

In general, crack width of concrete cover determines ongoing deterioration of an RC member. In addition, the end of service life of RC structures is normally defined as excessive cracking, *i.e.* when the width of a crack due to corrosion, w, exceeds a limit value, w_{lim} (e.g. w_{lim} = 0.5mm for serviceability limit state (Kashani, 2014)). To estimate the crack width due to corrosion, the following empirical Eq. (12), proposed by Vidal et al. (2004) is used :

$$w = K\left(\Delta A_s - \Delta A_{s0}\right) \tag{12}$$

where ΔA_s is the loss of the reinforcing bar cross section in mm^2, ΔA_{s0} is the steel cross section loss needed for crack initiation in mm^2, and K = 0.0575 is an empirical coefficient. The additional corrosion penetration, Δp_{lim}, corresponding to the limit crack width, w_{lim} can be estimated as follows (Val, 2007):

$$\Delta p_{lim} = \frac{D_0 - 2p_0}{2} - \sqrt{\left[\frac{D_0 - 2p_0}{2}\right]^2 - \frac{w_{lim}}{\pi K}} \tag{13}$$

where , p_0 is the corrosion penetration corresponding to ΔA_{s0} . Given Δp_{lim}, the time of failure, t_f , can be easily evaluated as follow:

$$t_f = \frac{\Delta p_{\lim} + 0.116 i_{corr0}(t_{cr} + T_{corr})}{0.116 i_{corr0}} \tag{14}$$

It should be noted that there is currently no recommendation in the literature regarding to the value of Δp_{lim} in terms of the residual capacity of the corroded RC component. This is

discussed in detail in section 4 of this paper.

3. Proposed finite element model of RC columns using nonlinear fibre beam-column element

In this research the nonlinear FE modelling technique using fibre beam-column element developed by Kashani et al. (2016a, 2016b) is employed. This modelling technique was calibrated and validated for circular RC columns bridge piers. Here, this model is extended to be used to simulate the nonlinear behaviour of rectangular RC columns. Therefore, it requires to be validated against experimental data of uncorroded and corroded rectangular RC columns.

As it is reported by other researchers (Coleman & Spacone, 2001; Pugh et al., 2015), in modelling nonlinear behaviour of RC structures, the softening type behaviour of RC components affects the simulation results due to strain localisation in critical section. To avoid strain localisation in the analyses, the regularisation technique suggested by Coleman and Spacone (2001) and Pugh et al.(2015) to predict the nonlinear response of RC shear walls, which has successfully been employed by Kashani (2014) in RC bridge piers is used. In this technique, to avoid strain localisation due to the post buckling response of reinforcing bars, the integration length of the critical section is considered to be equal to the buckling length. Using this approach the fracture energy under the post buckling response of the material model for reinforcing steel remains unchanged. Therefore, two force-based elements are used to model the RC column. The length of first element is considered to be twice of the buckling length of the vertical bars, $2L_{eff}$ (where L_{eff} is the buckling length) together with Newton-Cotes integration scheme with two integration points. For the second element, the Gauss-Lobatto integration scheme with 5 integration points is used. To model the strain penetration and slippage of reinforcements anchored to the foundation, a zero length section element is used (Berry & Eberhard, 2004). However, because reinforcement are anchored

well below the foundations, it is unlikely that they are corroded in that depth. Therefore, the uncorroded bond-slip model is used. Other researchers (Kallias and Imran 2010) reported that bond-slip degradation of corroded RC beams does not have any impact on residual capacity of these beams. Therefore, this aspect has not been considered here. However, bond-slip degradation is very important at the RC joints in frame structures (Lowes et al., 2005; Lowes et al.,2003). It should be noted that other researchers (Jeon et al., 2015) have used springs to model shear failure in RC columns. However, there is no stable fibre element formulation to model axial-flexure-shear interaction in RC components with and without the effect of corrosion. Therefore, in this study we focused on flexural failure only. The proposed fibre model is shown in Fig.2.

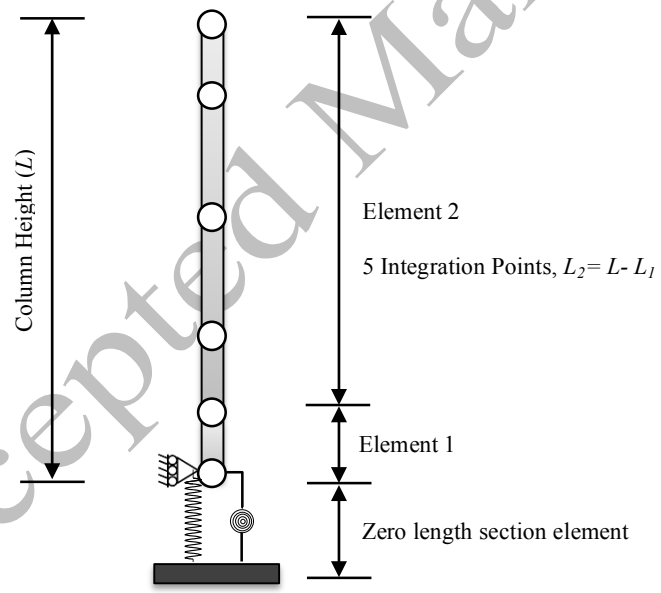

Fig. 2. The proposed nonlinear fibre beam-column model

3.1 Description of uniaxial material models

3.1.1 Unconfined and confined concrete models

The uniaxial material model, Concrete02 (Yassin, 1994), available in OpenSees is used to

simulate the behaviour of unconfined concrete. This material model employs a parabolic curve in pre-peak stress–strain response in compression, and employs a linear softening curve in post-peak response to a residual compressive strength, which is 20% of maximum strength. The stress–strain response in tension is a bilinear curve to a residual tensile strength of zero. To simulate the corrosion induced cracking and spalling of concrete cover due to accumulation of expansive rust products, the following approach suggested by Coronelli and Gambarova (2004) is used:

$$\sigma_c^{'} = \frac{\sigma_c}{1 + K_1 \frac{\varepsilon_1}{\varepsilon_{c0}}} \tag{15}$$

where, σ'_c is the residual compressive strength of cracked concrete cover, σ_c is the compressive strength of the sound cover concrete, K_1 is the bar roughness and diameter which can be taken as $K = 0.1$, ε_{c0} is strain corresponding to the peak compressive stress σ_c; and ε_1 is average tensile strain of the cracked concrete which is calculated using the following equations:

$$\varepsilon_1 = \frac{(P_{corr} - P_0)}{P_0} \tag{16}$$

$$P_{corr} - P_0 = n_{bars} w_{cr} \tag{17}$$

$$w_{cr} = 2\pi(\nu_{rust} - 1) P_{ave} \tag{18}$$

where, P_0 is the perimeter of the uncorroded column section, P_{corr} is the perimeter of the corroded column section, n_{bars} is the number of bars in column section, w_{cr} is the total crack width for a given corrosion level P_{ave}. ν_{rust} is ratio of the volumetric expansion of the corrosion products with respect to the uncorroded steel (the suggested value is $v_{rs} = 2$). According to modified Kent and Park model (Scott et al., 1982), to consider confinement effect, compressive strength of core concrete and its corresponding strain are increased by factor of K_c. This factor is calculated as follows:

$$K_c = 1 + \frac{\rho_s \sigma_{yh}}{\sigma_c} \tag{19}$$

where, σ_{yh} is yield strength of steel hoops and ρ_s is the volumetric ratio of the rectangular steel hoops to the volume of concrete core measured to the outside of the peripheral hoop. Previous research by Kashani et al. 2016b revealed that Mander's model works perfectly fine for circular cross sections, but significantly over estimate the confinement level for rectangular/square cross sections. The parametric studies conducted by Pugh et al. (2015) and Salami (2017) showed that, the simple Eq. (19) works much better for rectangular and square cross sections.

When corrosion of tie reinforcements starts, cross sectional area, yield strength and fracture strain of ties decreases over time. So, to take into account the effects of corrosion, σ_{yh} and ρ_s should be substituted by $\sigma_{yh}(t)$ and $\rho_s(t)$, respectively:

$$\sigma_{yh}(t) = \left[1 - 0.005\psi_{tie}(t)\right]\sigma_{yh} \tag{20}$$

$$\rho_s(t) = \left[1 - 0.01\psi_{tie}(t)\right]\rho_s \tag{21}$$

where, $\sigma_{yh}(t)$, $\rho_s(t)$ and $\psi_{tie}(t)$ are yield strength, volumetric ratio of the rectangular steel ties, and time-dependent percentage of mass loss of the corroded ties at time t after corrosion initiation, respectively. Using Eqs. (20) and (21), the confinement factor, K_c, is modified.

The compression strain of confined concrete at fracture of first horizontal tie reinforcement, ε_{cu}, is modified as follows to account corrosion effects (Priestley & Paulay, 1992).

$$\varepsilon_{cu}(t) = 0.004 + 1.4\left[\frac{\rho_s(t)\sigma_{yh}(t)\varepsilon_{uh}(t)}{\sigma_{cc}(t)}\right] \tag{22}$$

where, σ_{cc} is time-dependent compressive strength of confined concrete and $\varepsilon_{uh}(t)$ is time-dependent transverse steel strain at maximum steel stress. According to Du et al. (2005a,

2005b), $\varepsilon_{uh}(t)$ can be obtained as follows:

$$\varepsilon_{uh}(t) = \left[1 - 0.05\psi_{tie}(t)\right]\varepsilon_{uh} \quad (23)$$

where ε_{uh} is strain at maximum stress of uncorroded transverse steel.

3.1.2 Reinforcing steel model

The uniaxial material model developed by Kashani et al. (2015a) is used to model the nonlinear stress-strain behaviour of reinforcing bars in tension and compression. This model accounts for reduction in yielding stress and ductility of reinforcing steel in tension due to pitting corrosion using the empirical models recommended by Du et al. (2005a, 2005b). Kashani et al. (2015a) model is capable of simulating the post-buckling behaviour of reinforcing bars in compression considering the effect of corrosion. To consider the effect of corrosion on low-cycle fatigue behaviour of corroded bars, the Coffin-Manson (Manson,1965) model, modified by Kashani et al. (2015b, 2013a), is used. Further details about the model development are available in (Kashani et al., 2015a).

3.2 Verification of the nonlinear finite element model using experimental data

Here the experimental results of reaction wall tests on corroded and uncorroded rectangular RC columns by Meda et al. (2014) is used to verify the proposed nonlinear FE model. They tested an uncorroded control specimen, and a corroded column with about 20% average mass loss under cyclic loading. It should be noted that in their experimental study, only longitudinal reinforcing bars were corroded and the stirrups were protected from corrosion through a suitable paint. The geometry and details of their tested RC column specimen is shown in Fig. 3.

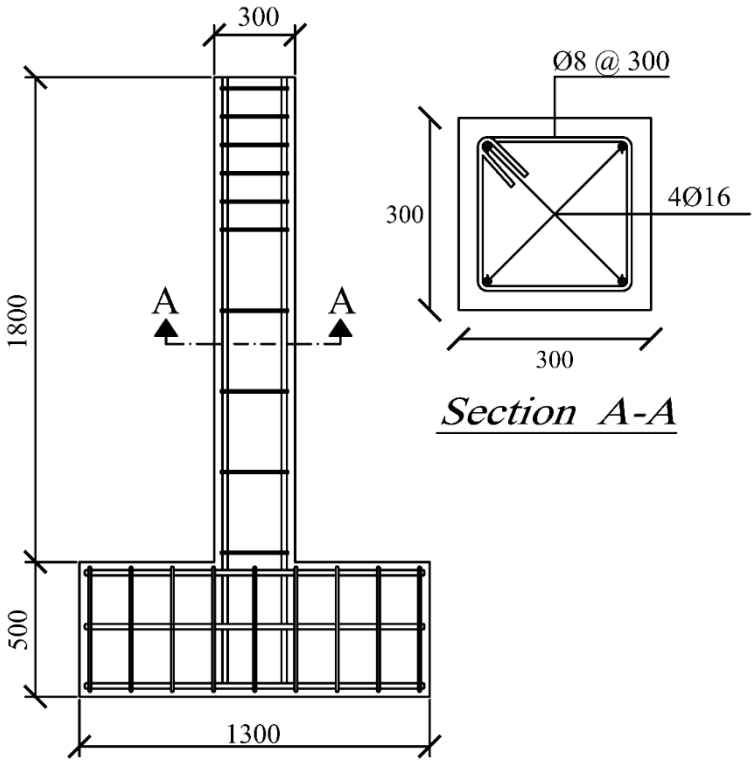

Fig. 3. Details of the column tested by Meda et al. (2014)

Fig. 4 shows the comparison of the hysteresis loops between the numerical analysis and the experimental data of uncorroded RC column. As it is shown in Fig. 4, the proposed FE model can accurately simulate the nonlinear response of uncorroded column, and the numerical simulation is in good agreement with the experimental results. In order to demonstrate the importance of considering the buckling behaviour of corroded reinforcements, the simulation results of the corroded column are presented in two cases, with and without considering buckling of reinforcing bars. For the latter, the conventional steel02 model (Giuffre–Menegotto–Pinto model (Menegotto, 1973)) available in the OpenSees is used, which considers the same behaviour for tension and compression. In Fig. 5 (a) and (b), simulation results of the corroded column are shown in two cases of using Steel02 model and buckling model, respectively. It can clearly be seen in Fig.5 (a) that although the lateral load resistance and initial stiffness of the column are well predicted, cyclic degradation and capacity loss (R_{loss}) of the column due to buckling of vertical bars

cannot be captured using Steel02. However, cyclic degradation and capacity loss of the column can be simulated realistically in the model accounting for buckling of vertical bars (Fig. 5(b)). This shows that the energy dissipation capacity of corroded RC components, which is one of the main characteristics of the structures located in high seismicity regions, reduces significantly due to the combined effects of inelastic buckling, corrosion, and low-cycle fatigue degradation. The accuracy of the FE model is check using hysteretic force error, E_{force}, and hysteretic energy error, E_{energy} (Eqs. (24) and (25)).

$$E_{force} = \sqrt{\frac{\sum_{i=1}^{n} (F_{meas}^{i} - F_{calc}^{i})^2}{n\,(max(F_{meas}))^2}} \tag{24}$$

$$E_{energy} = \frac{\Omega_{meas} - \Omega_{calc}}{\Omega_{meas}} \tag{25}$$

where F_{meas} and F_{calc} are the measured and calculated lateral forces at corresponding peak displacements, and n is the number of peak points in the loading history; Ω_{meas} and Ω_{calc} are the measured and calculated areas within the hysteresis loops which can be calculated using the Green's theorem (Kahsani et al 2016b). In Table 2, the values of hysteresis energy and force error are tabulated. The cumulative dissipated hysteresis energy for uncorroded and corroded columns are also shown in Fig. 6 (a) and (b). It should be noted that in Fig 6, all of calculated energy dissipation values are normalised to total dissipated energy of experimental testing of uncorroded column.

Table 2. Quantitative comparison of the error in computational model

Specimen	E_{force} (%)	E_{energy}(%)
Uncorroded Column	8.54	-20.58
Corroded Column	6.98	-15.61

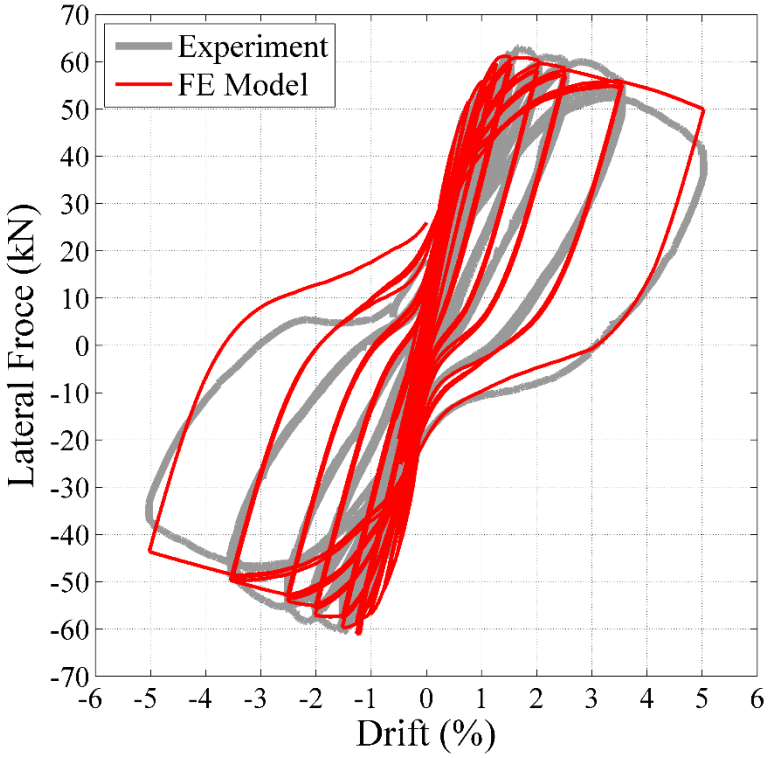

Fig. 4 Verification of the uncorroded column FE model

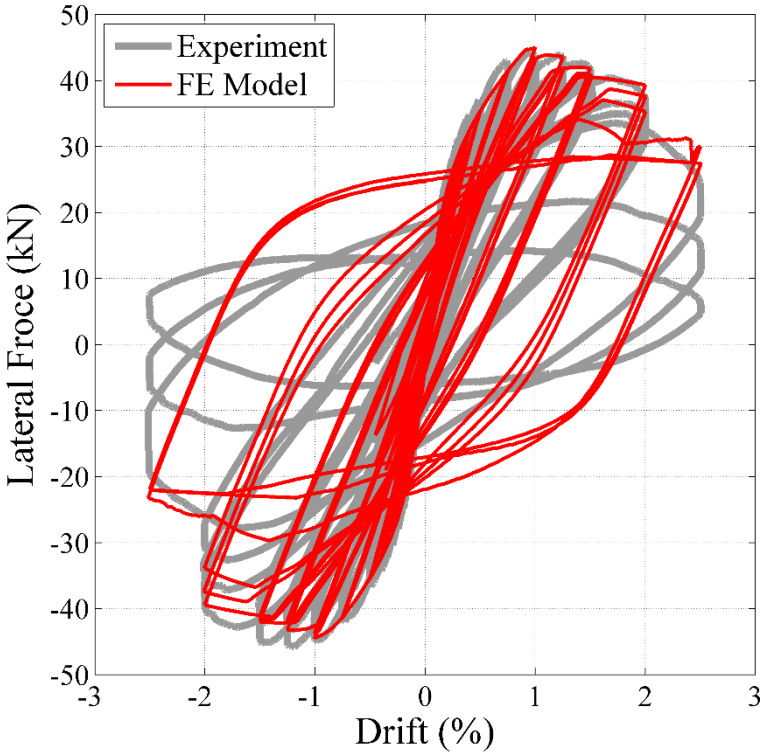

(a)

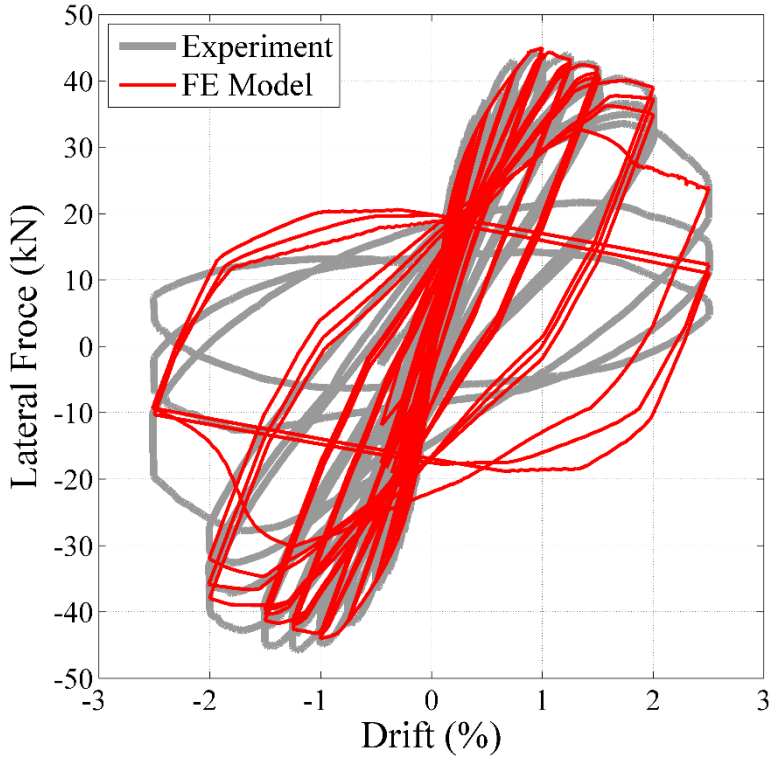

(b)

Fig. 5 Verification of the corroded column FE model: (a) using Steel02 model, (b) using buckling model

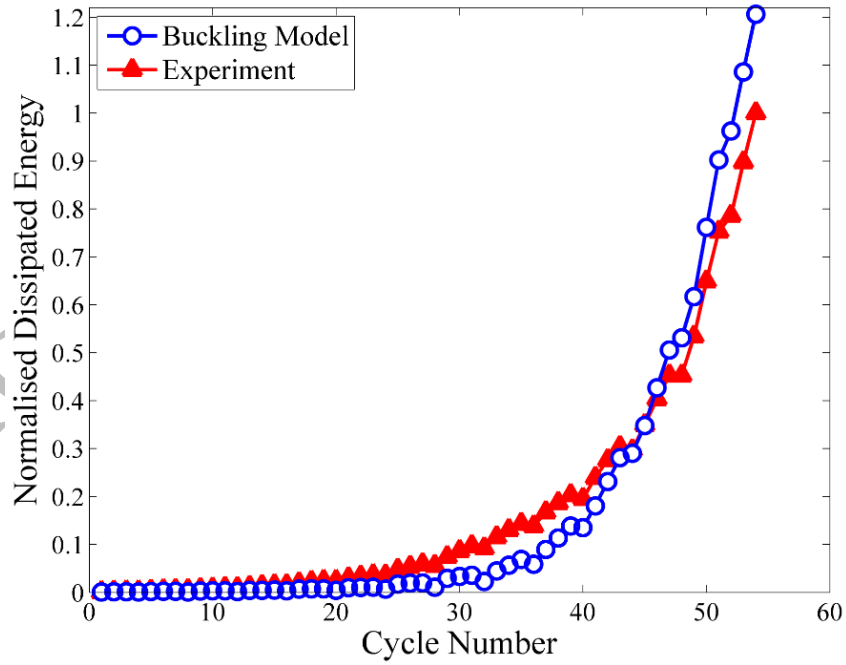

(a)

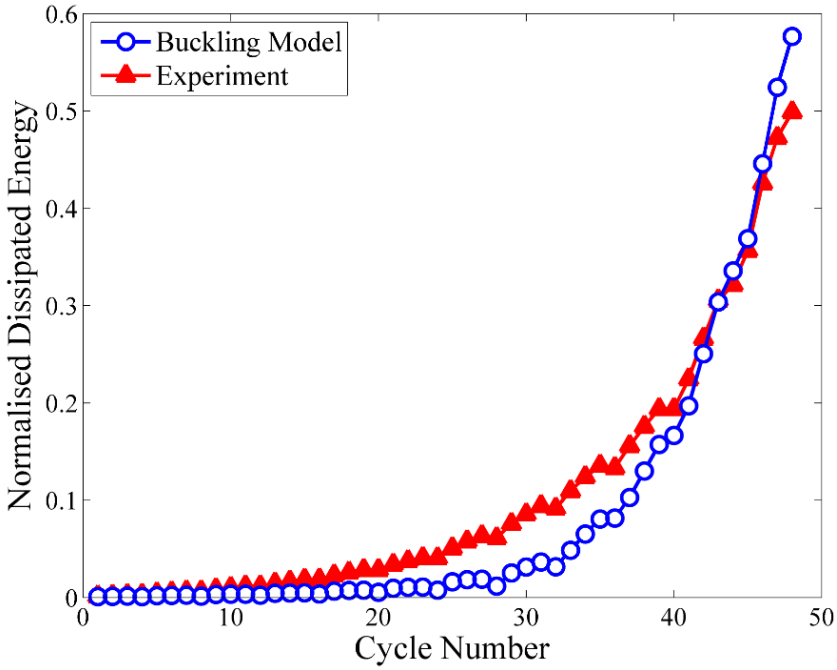

(b)

Fig 6. Cumulative dissipated energy versus cycle number; (a) uncorroded column and (b) corroded column

4. 3D time-dependent capacity surface and damage limit states of corroded RC columns

In this section, the verified FE model is extended for a parametric study to investigate the time-dependent capacity of two hypothetical columns, namely column A and column B. The proposed column is 1500 mm in height and 250 mm square cross section. Fig. 7 shows the details of proposed columns cross section. The columns cross sections include 8 vertical reinforcing bars of 16 mm diameter, and the diameter of horizontal tie reinforcement is 8 mm (this represents the RC columns in building structures). The only difference between column A and column B is in the spacing of horizontal ties. The horizontal ties spacing of column A is 80 mm and column B is 200 mm. The mechanical properties of vertical and horizontal tie reinforcement are summarised in Table 3. The concrete compressive strength is considered to be 30 MPa. To investigate the effect of corrosion on time-dependent displacement ductility

and flexural capacity loss (R_{loss}) of corroded RC columns, different degrees of corrosion (i.e. mass loss ratios) at 5 year intervals are considered. To include the axial force effects, analyses are conducted for varied axial force ratios [0, 0.1, 0.2, 0.3 and 0.4 (N_u /$\sigma_c A_c$)], where N_u is the axial force, σ_c is the compressive strength of concrete and A_c is the gross cross section area of column cross section. It is worth mentioning that corrosion of horizontal ties is also considered in these analyses.

Table 3 Mechanical properties of test specimens

Bar Diameter		**16 mm**	**8 mm**
Yield strain	ε_y	0.00252	0.00247
Yield stress (MPa)	σ_y	530	510
Elastic modulus (MPa)	E_s	210000	212099
Hardening strain	ε_{sh}	0.0083	No plateau
Strain at maximum stress	ε_u	0.06	0.06033
Maximum stress (MPa)	σ_u	630	616
Fracture strain	ε_r	0.18	0.161

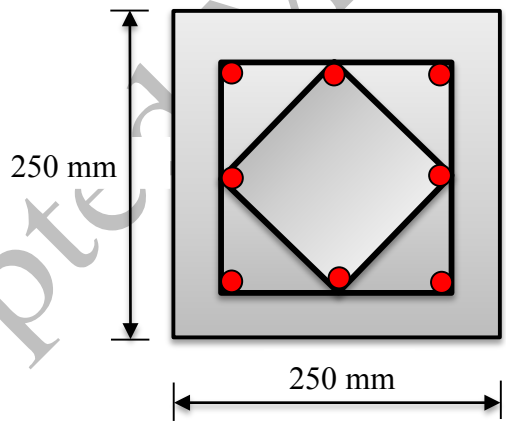

Fig. 7 Hypothetical columns section

4.1 Analyses results and discussion

4.1.1 Nonlinear behaviour, failure modes, and 3D time-dependent capacity surface of corroded columns

To investigate the impact of corrosion and axial load on capacity and ductility of RC columns (damage limit states), a series of time-dependent nonlinear pushover analyses with various

corrosion levels are conducted.

Fig. 8 shows the results of monotonic pushover analyses. According to Fig. 8(a), for axial force ratio of 0.1, the failure mechanism of the column A for up to approximately 20% mass loss is core concrete crushing in compression. However, for corrosion levels beyond 20% mass loss the failure mode changes from concrete crushing in compression to combined core concrete crushing followed by bar fracture in tension. As it is shown in Fig.8 (b), increasing the axial force ratio to 0.3, results in a rapid reduction in flexural capacity and ductility of corroded column compared to the previous cases. Moreover, when the axial force ratio is 0.3, approximately up to 24% mass loss the failure mode is governed by core concrete crushing (more brittle failure mode). According to Fig.8 (c-d), for the same axial load and corrosion levels, failure mode of column B is governed mainly by core concrete crushing. Especially, when the axial load ratio is 0.3 and rapid flexural capacity and ductility loss is seen due to premature buckling, followed by core concrete crushing in column B (Fig.8 (d)). This is due to lack of confinement in the column B in comparison with the column A.

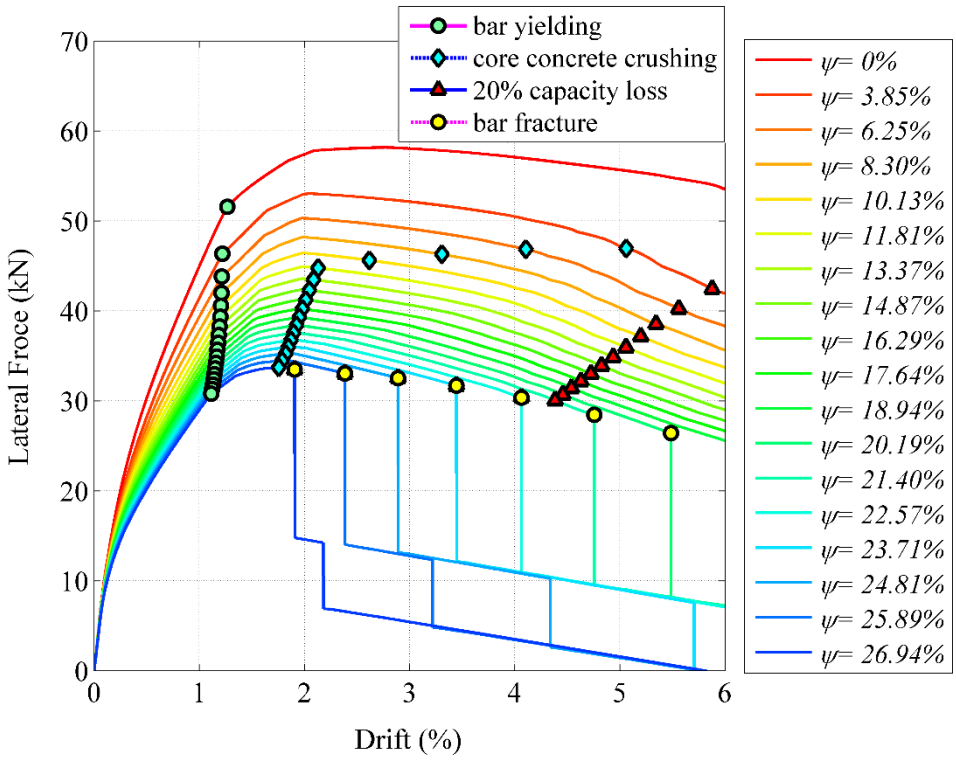

(a)

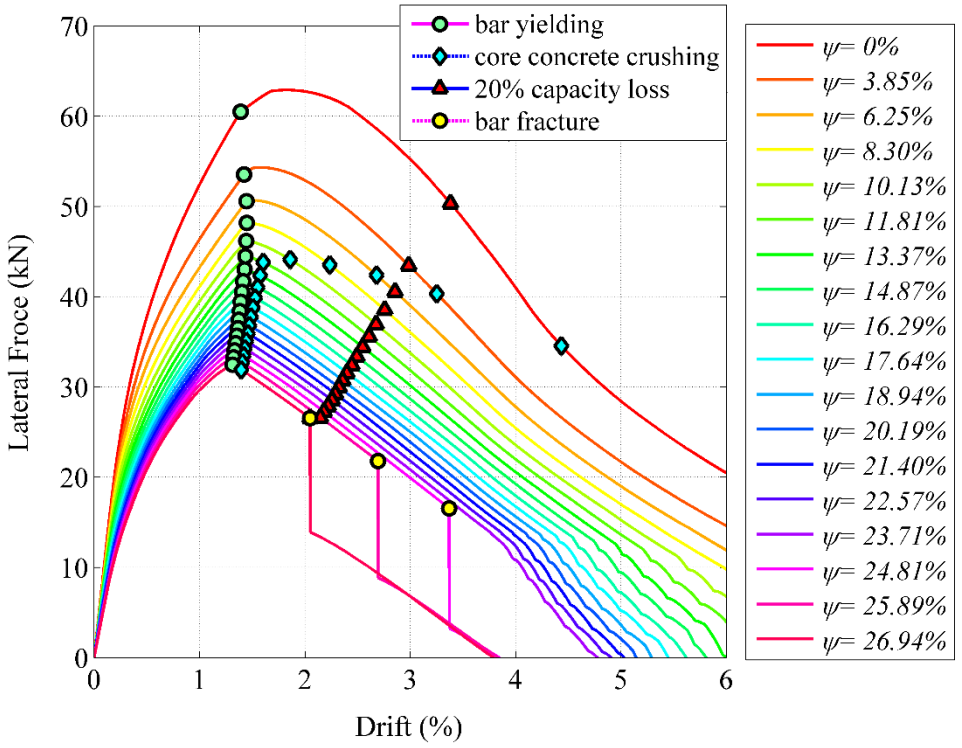
bar yielding
core concrete crushing
20% capacity loss
bar fracture
ψ= 0%
ψ= 3.85%
ψ= 6.25%
ψ= 8.30%
ψ= 10.13%
ψ= 11.81%
ψ= 13.37%
ψ= 14.87%
ψ= 16.29%
ψ= 17.64%
ψ= 18.94%
ψ= 20.19%
ψ= 21.40%
ψ= 22.57%
ψ= 23.71%
ψ= 24.81%
ψ= 25.89%
ψ= 26.94%
Lateral Froce (kN)
Drift (%)
0
10
20
30
40
50
60
70
0
1
2
3
4
5
6

(b)

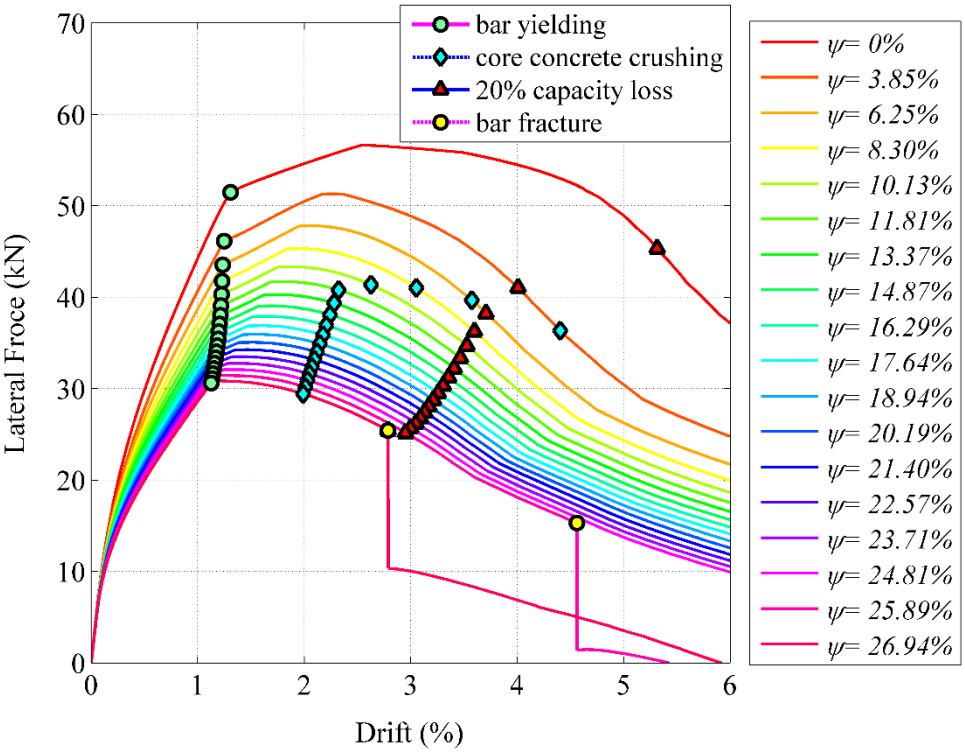
bar yielding
core concrete crushing
20% capacity loss
bar fracture
ψ= 0%
ψ= 3.85%
ψ= 6.25%
ψ= 8.30%
ψ= 10.13%
ψ= 11.81%
ψ= 13.37%
ψ= 14.87%
ψ= 16.29%
ψ= 17.64%
ψ= 18.94%
ψ= 20.19%
ψ= 21.40%
ψ= 22.57%
ψ= 23.71%
ψ= 24.81%
ψ= 25.89%
ψ= 26.94%
Lateral Froce (kN)
Drift (%)
0
10
20
30
40
50
60
70
0
1
2
3
4
5
6

(c)

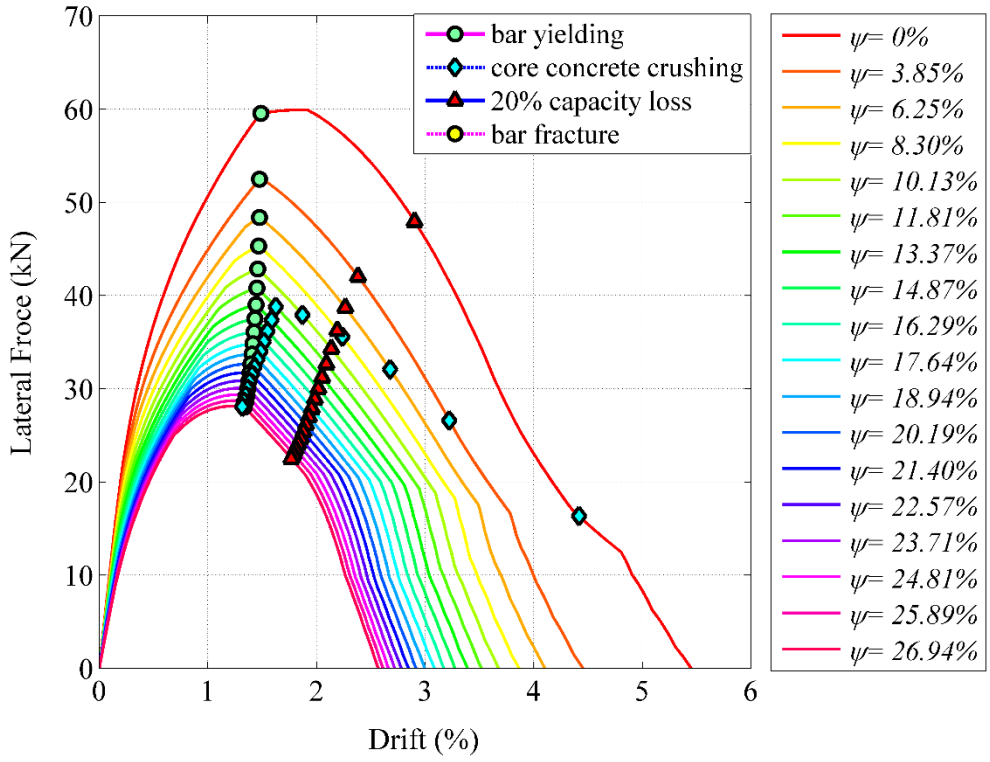

(d)

Fig. 8 Mass loss-dependent pushover analyses of corroded columns: (a) column A with axial load ratio of 0.1, (b) column A with axial load ratio of 0.3, (c) column B with axial load ratio of 0.1, and (d) column B with axial load ratio of 0.3

Fig. 9 shows some exemplary contour plots of 3D time-dependent capacity surfaces of the columns A and B for 0.1 and 0.3 axial force ratios. The failure lines (as identified in pushover curves in Fig. 8) are also mapped on the contour plots to show the failure regions over time. The Fig. 9 (a) shows that in case of 0.1 axial force, from approximately 20% mass loss, failure mode of column A changes from core concrete crushing in compression, to combined core concrete crushing followed by bar fracture in tension. However, based on Fig. 9 (c), for same axial force, up to 26% mass loss, the failure mode of column B is governed by concrete crushing in compression and beyond 26% mass loss is core concrete crushing followed by bar fracture. Fig. 9 (b) shows that for 0.3 axial force ratio, after about 25%mass loss, the failure mode of column A changes from core concrete crushing in compression, to combined core concrete crushing followed by bar fracture in tension. However, for 0.3 axial

force ratio, the failure mode of column B is core concrete crushing in compression (Fig.9 (d)).

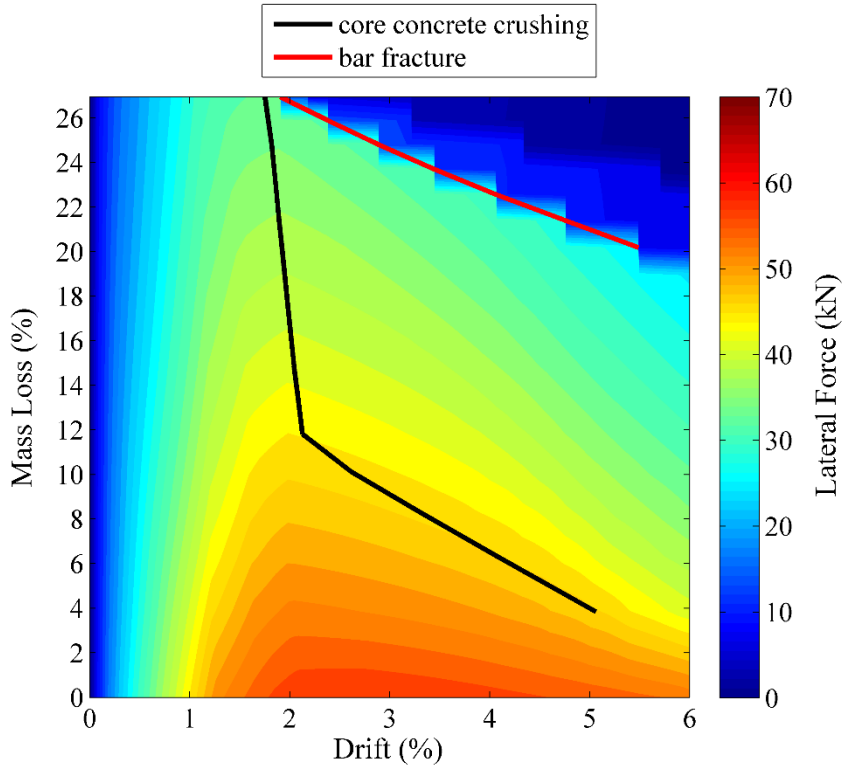

(a)

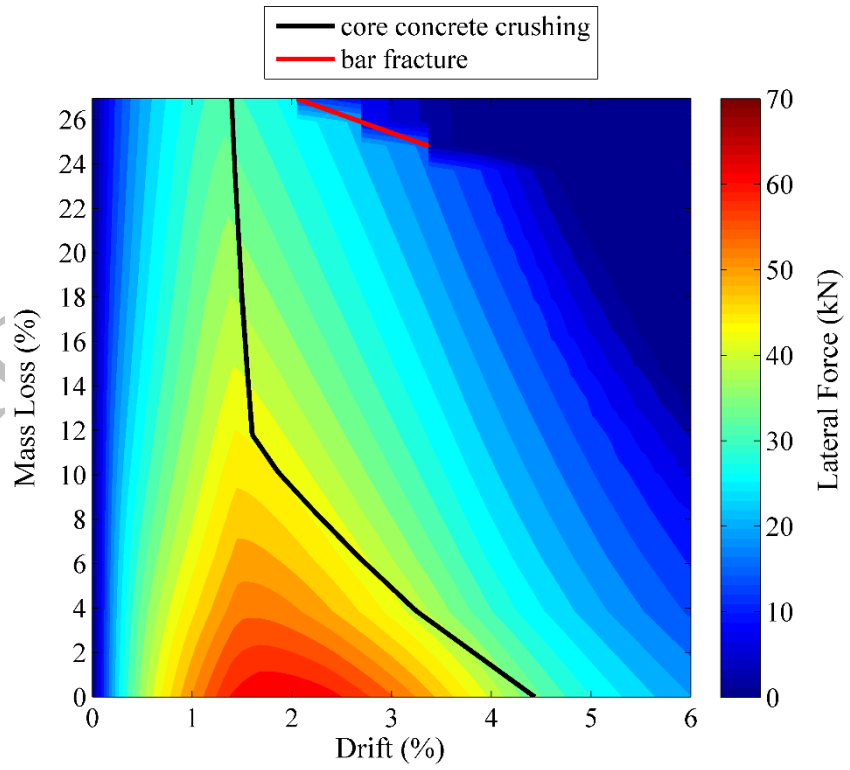

(b)

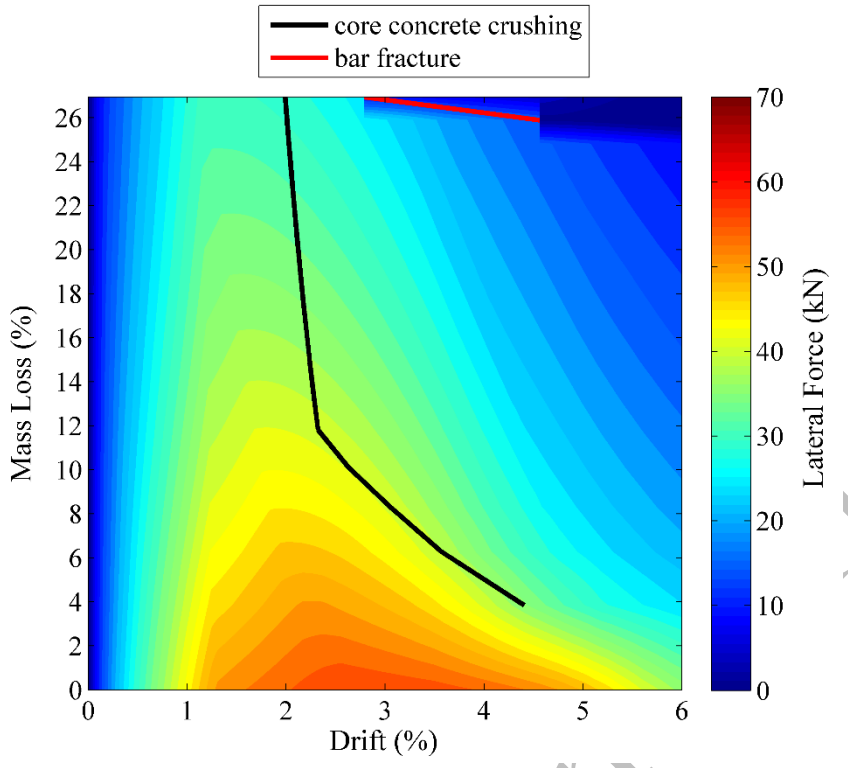

(c)

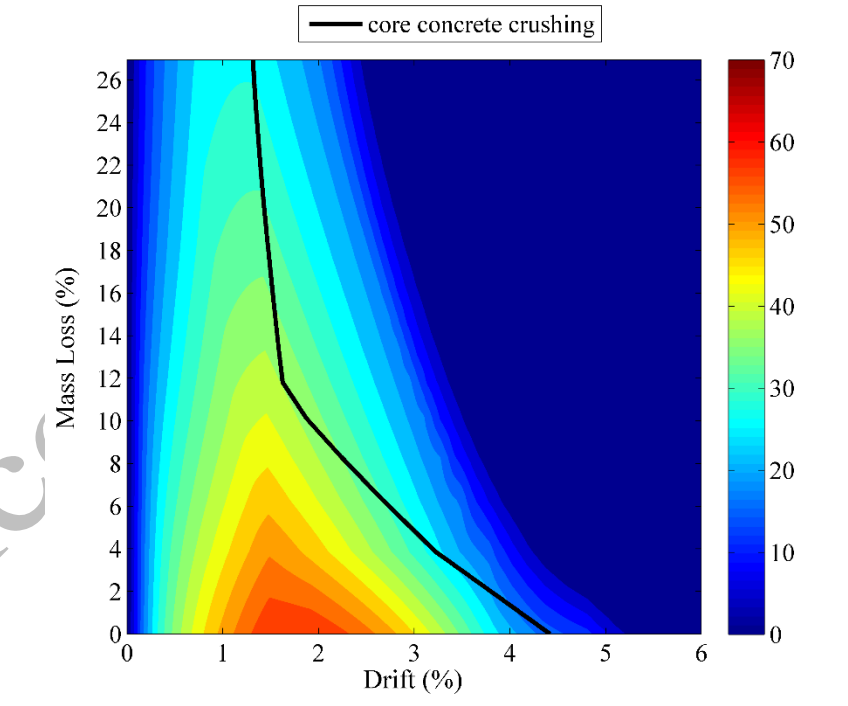

(d)

Fig.9 3D capacity contours of columns A and B: (a) column A with axial force ratio = 0.1, (b) column A with axial force ratio = 0.3, (c) column B with axial force ratio = 0.1, and (d) column B with axial force ratio = 0.3

4.2 Impact of corrosion on damage limit states

In this section, the significance of combined effects of axial force and corrosion damage on ductility and capacity of corroded columns are quantified. The ductility factor μ, is considered as the ratio between the ultimate displacement (Δu) and yielding displacement (Δy). There are several definitions for Δu and Δy in literature [68-70], but all of them are related to uncorroded columns and are not suitable for corroded columns. In this study, Δy is considered as the lateral displacement associated with the yielding of reinforcing steel in tension. The Δu is considered as the smallest value of three criterions: (*i*) lateral displacement at fracture of reinforcing bars in tension, (*ii*) lateral displacement at crushing of core concrete (Eq.(22)), and (*iii*) lateral displacement at 20 % column's flexural capacity loss. These parameters are known as damage limit states (Berry & Eberhard, 2004, 2005; Kowalsky, 2000), and are used in fragility analysis of RC structures subject to earthquake loading. However, corrosion changes these parameters over time. This section shows that the proposed nonlinear FE framework developed in this paper, can accurately quantify the impact of corrosion on damage limit states of RC columns.

Fig.10 shows the influence of corrosion and concrete cover cracking on normalised capacity (E_R) of the corroded columns. The normalised capacity is the ratio of flexural capacity of corroded column to flexural capacity of uncorroded column. From the analysis results, it is clear that column B has more severe reduction in capacity with increasing mass loss. This is due to lack of confinement reinforcement in column B in comparison with column A. For 20% mass loss and 0.2 axial force ratio, capacity loss of column B is about 35%, which is in good agreement with experimental results observed by Meda et al.(2014). The capacity loss observed in the experiment in (Meda, et al., 2014) is slightly less than the computed capacity loss in the current study. This is because that they prevented the corrosion of horizontal tie reinforcements while in the current study, the corrosion of horizontal ties is

included. Fig. 10(b) shows that 0.5 mm crack width [this is suggested to be the end of service life of corroded structures by other researchers (Val, 2007)] results in approximately 15% to 25% reduction in the flexural capacity of columns, depending on the axial force ratio. However, Fig. 10(d) shows that 0.5 mm crack width on column B with axial force ratio of 0.4, results in about 30 % flexural capacity loss. (Ghosh & Sood, 2016) suggested to consider 1.0 mm crack width as the critical serviceability limit state for concrete cover spalling. However, considering 1.0 mm crack width shows that the flexural capacity reduction of columns will be varied from 20 % to 40 % depending on the axial force ratio.

Fig. 11 shows the influence of corrosion and concrete cover cracking on normalised ductility factor (E_μ) of the corroded columns. The normalised ductility factor is the ratio of ductility factor of corroded column to ductility factor of uncorroded column. Fig. 11(c) shows that 20% mass loss and axial force ratio of 0.2, reduces the ductility of a corroded column by about 50%. This is in good agreement with experimental results observed by other researchers (Meda et al., 2014; Li et al., 2015). This confirms that corrosion has more significant impact on ductility loss of RC components than flexural capacity loss. Fig 11(b) and (d) shows that 0.5 mm crack width results in 20% to 40% ductility loss, depending on the axial force ratio, in the column A. Considering 1.00 mm crack width, the ductility loss will increase to up to about 60 % in column A. Column B shows a similar behaviour with a slightly less ductility loss.

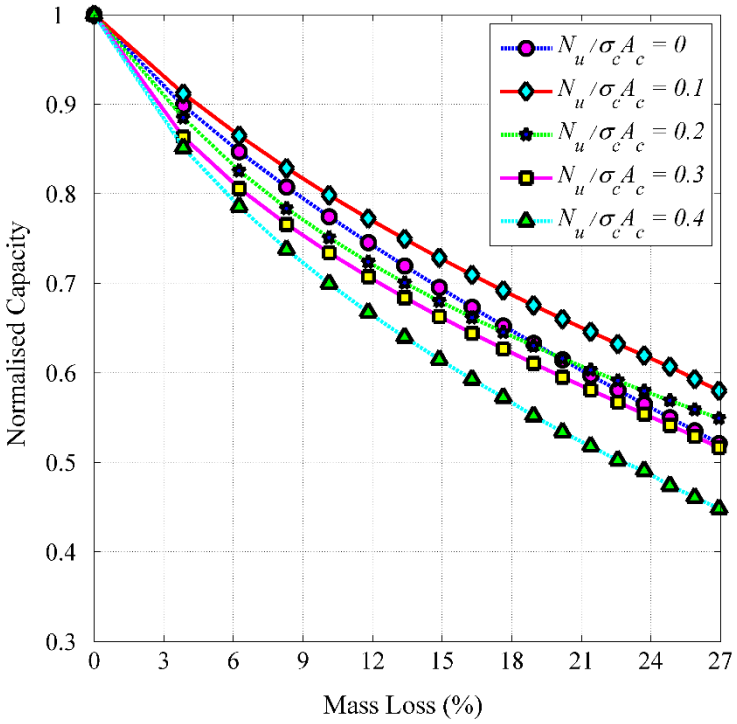
Normalised Capacity
Mass Loss (%)
$N_u/\sigma_c A_c = 0$
$N_u/\sigma_c A_c = 0.1$
$N_u/\sigma_c A_c = 0.2$
$N_u/\sigma_c A_c = 0.3$
$N_u/\sigma_c A_c = 0.4$

(a)

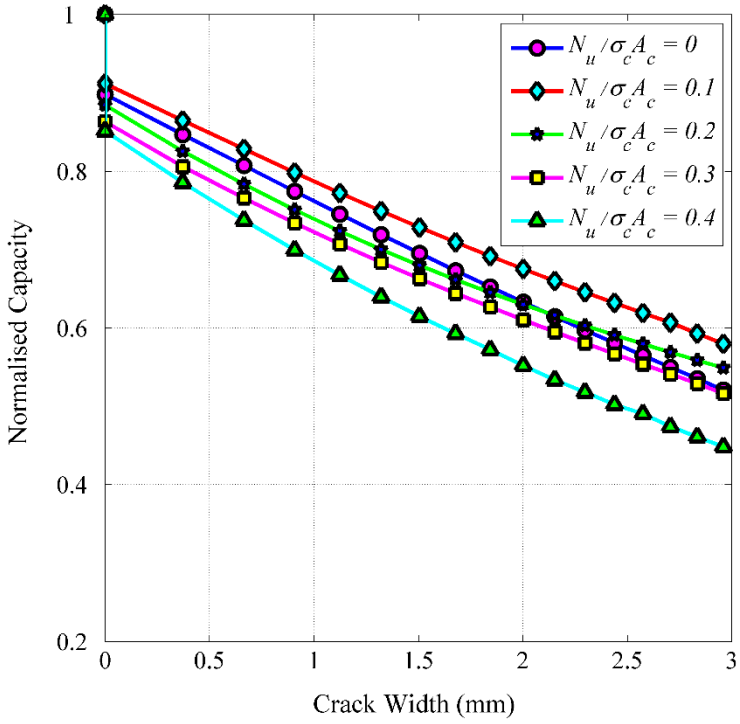
Normalised Capacity
Crack Width (mm)
$N_u/\sigma_c A_c = 0$
$N_u/\sigma_c A_c = 0.1$
$N_u/\sigma_c A_c = 0.2$
$N_u/\sigma_c A_c = 0.3$
$N_u/\sigma_c A_c = 0.4$

(b)

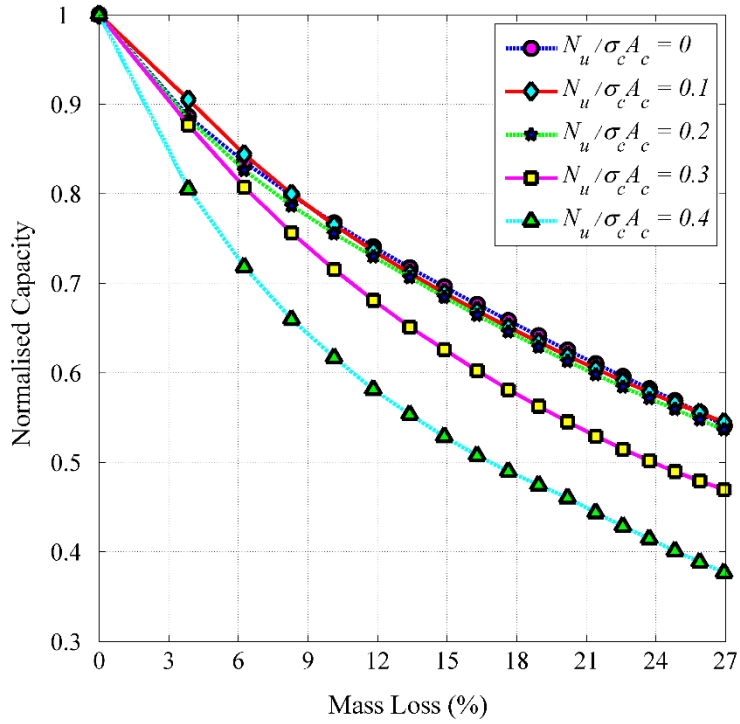

(c)

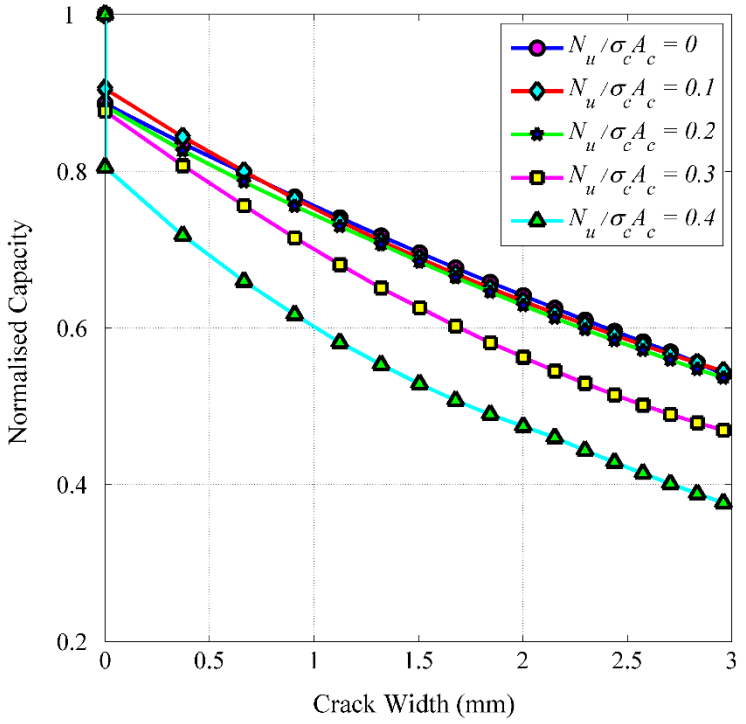

(d)

Fig. 10 Influence of mass loss and concrete cover cracking on flexural capacity loss of corroded columns with varied axial force ratios: (a) and (b) column A, and (c) and (d) column B

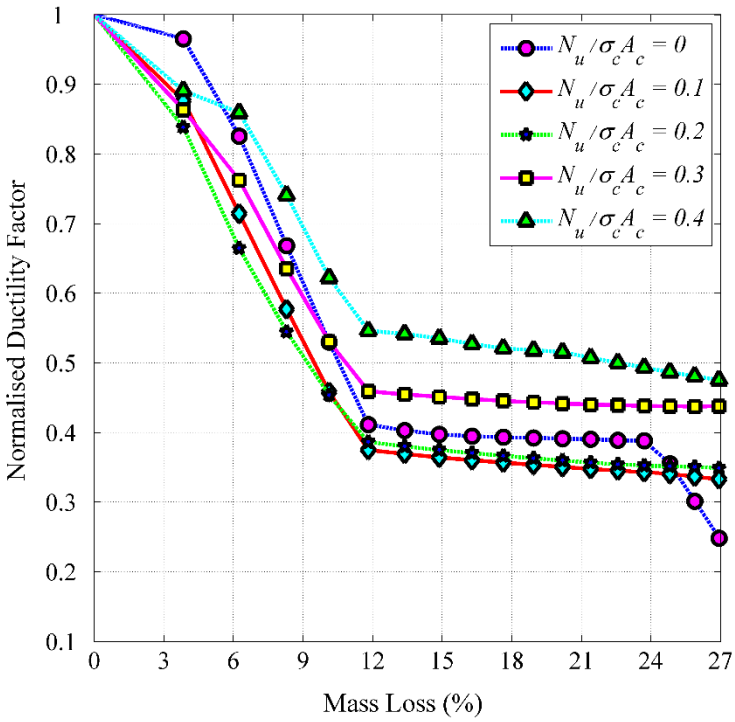
Normalised Ductility Factor
Mass Loss (%)
$N_u/\sigma_c A_c = 0$
$N_u/\sigma_c A_c = 0.1$
$N_u/\sigma_c A_c = 0.2$
$N_u/\sigma_c A_c = 0.3$
$N_u/\sigma_c A_c = 0.4$

(a)

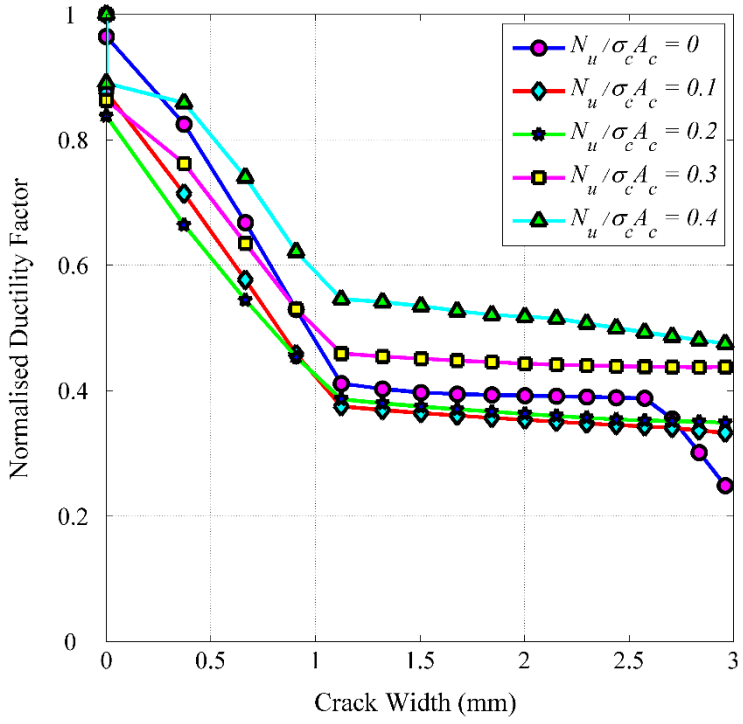
Normalised Ductility Factor
Crack Width (mm)
$N_u/\sigma_c A_c = 0$
$N_u/\sigma_c A_c = 0.1$
$N_u/\sigma_c A_c = 0.2$
$N_u/\sigma_c A_c = 0.3$
$N_u/\sigma_c A_c = 0.4$

(b)

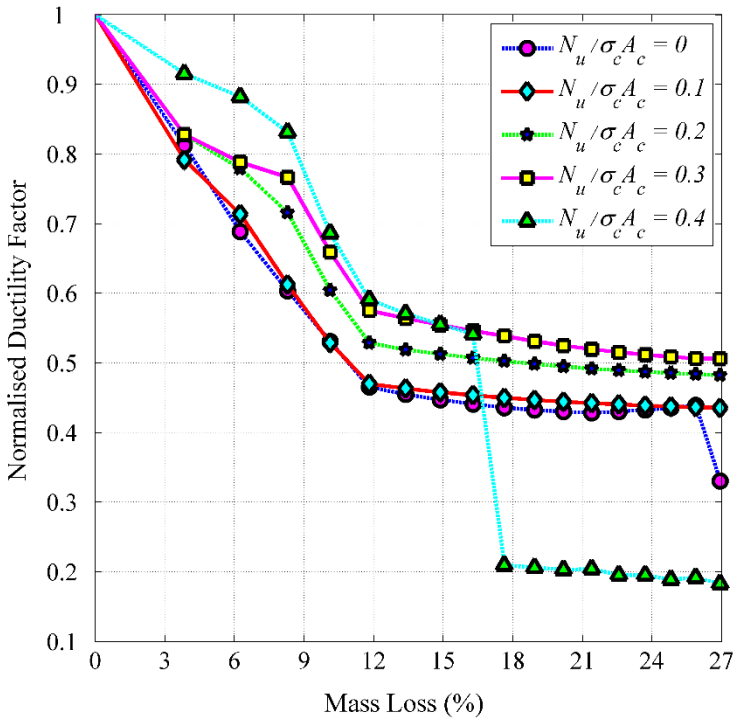

(c)

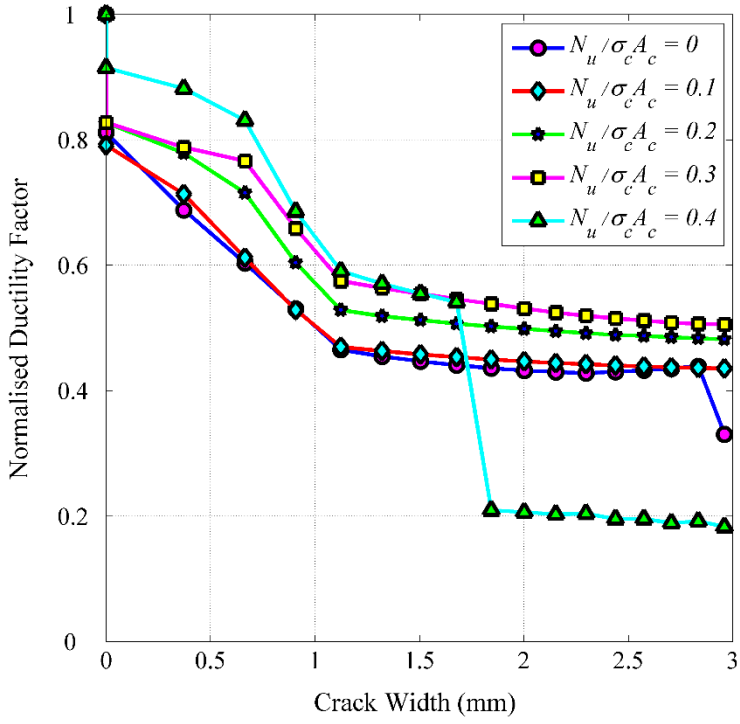

(d)

Fig. 11 Influence of mass loss and concrete cover cracking on ductility loss of corroded columns with varied axial force ratios: (a) and (b) column A, and (c) and (d) column B

The analyses results suggest that 0.5 mm crack width criterion which determines the end of service life of the RC structures (Val, 2007) results in about 15% reduction in flexural capacity of the columns. Other researchers (Barrera et al., 2012; Li et al., 2015) suggest the corresponding displacement to 15-20% flexural capacity loss as ultimate displacement of the structure. This shows that, the 0.5 mm crack width criteria for service life purposes is not a safe criteria, as the structure has already lost about 15% of its capacity. This is an area for further research and requires more detailed investigation using 3D continuum finite element technique.

5. Application of the proposed framework in nonlinear dynamic and seismic vulnerability analysis

In this section we show the application of the proposed framework in seismic collapse capacity assessment of corroded structures. Exemplary incremental dynamic analyses (IDAs) (Vamvatsikos & Cornell, 2002) on column A and column B, using Kobe ground motion, are performed. For each column, two percentage of mass losses of 10% and 20% are considered. The IDA curves of column A are shown in Fig. 12 and IDA curves of column B are shown in Fig. 13. The damage limit states for low-rise concrete moment frame with high code seismic design level defined in HAZUS (FEMA, 1999) are considered here to demonstrate the impact of corrosion on damage limit states.

The damage limit states described in HAZUS (FEMA, 1999) are not time-variant criterions, and do not account for material ageing. However, as described in section 4.1, corrosion changes the failure mechanism and also reduces the ductility of RC structures over their service life. Although in previous studies (Choine et al., 2013;Ghosh & Sood, 2016) fragility analyses are conducted for corroded structures, but they did not consider any change in damage limit states due to corrosion, and they used the same damage limit states related to

uncorroded structures. In order to develop a realistic analytical fragility function for corroded structures, the damage limit states should be modified to account for the corrosion effects.

In Fig. 12 and Fig 13 the uncorroded damage limit states of uncorroded columns are shown based on HAZUS recommendations for extensive and complete damage limit states. The extensive damage limit state is the drift ratio (drift ratio is the ratio of lateral tip displacement of the column to column height) at which concrete cover is spalled off, and reinforcement in tension is yielded. The complete damage limit state is the drift ratio corresponding to collapse of the column. It should be noted that the slight and moderate damage limit states are not applicable for corroded columns. This is because the corroded columns are already damaged, and slight and moderate damage limit states occur at very small drifts. The actual damage limit states of the corroded columns in Fig. 12 and Fig. 13 are considered using the pushover analysis procedure that explained in section 4 of this paper. As it is shown in Fig. 12 and Fig. 13, due to the impact of corrosion columns, damage limit states reach at smaller drift ratios in comparison with uncorroded columns.

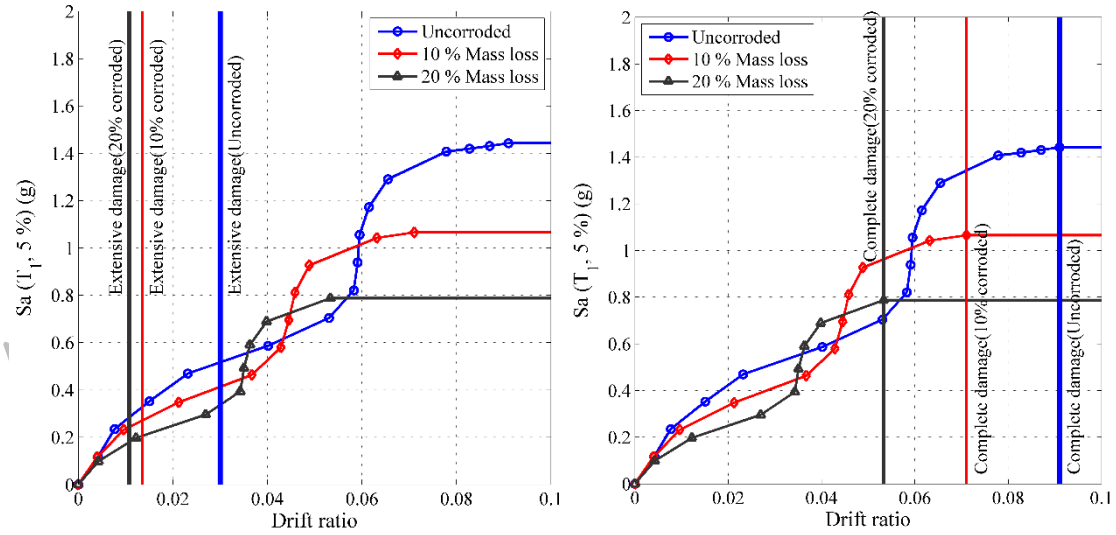

(a) **(b)**

Fig. 12 IDA results of column A and effect of corrosion on damage limit states: (a) extensive damage limit state, and (b) complete damage limit state

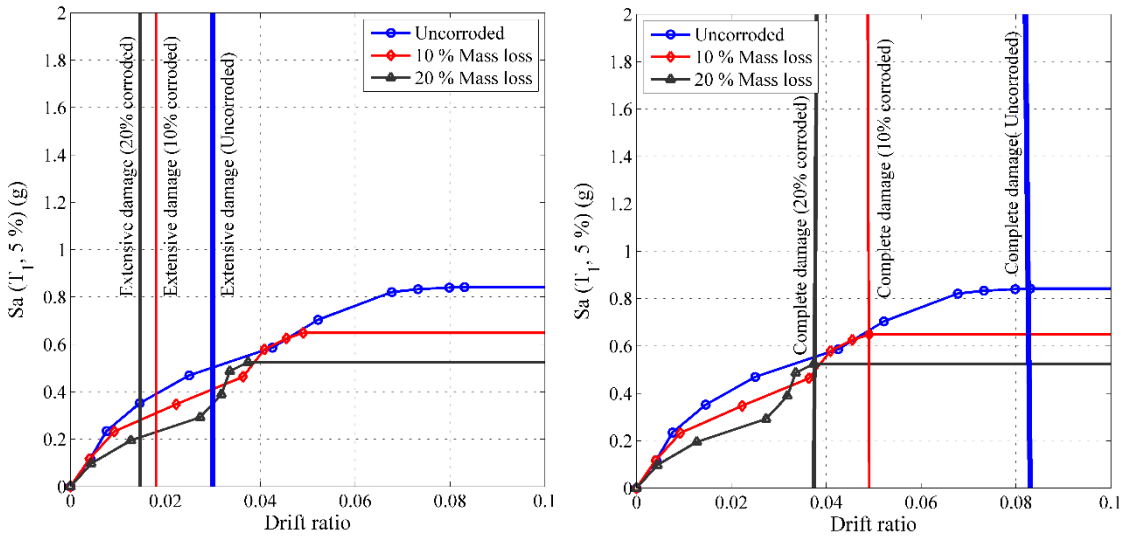

(a) **(b)**

Fig. 13 IDA results of column B and effect of corrosion on damage limit states: (a) extensive damage limit state, and (b) complete damage limit state

6. Conclusion

A computational platform for time-dependent capacity assessment of corroded RC structures using nonlinear FE analysis is developed. The proposed nonlinear FE model includes the impact of corrosion on inelastic buckling and low-cycle fatigue degradation of longitudinal reinforcement. The FE models of the corroded and uncorroded columns are verified against experimental results. The verification results show that when the effects of buckling and low-cycle fatigue degradation of reinforcing bars are included, the simulation results are in good agreement with the observed experimental results. The validated FE model is extended to conduct a parametric study on time-dependent capacity assessment of two hypothetical RC columns, varied in axial force ratios, mass loss ratios, cover crack widths, and confinement levels. The main findings of this research can be summarised as follows:

- For low axial force ratios, corrosion changes the failure mechanism of well confined column A from fracture of bars in tension (uncorroded column) to combined core concrete crushing followed by bar fracture in tension. For high

axial forces, the failure mechanism of column A is governed by core concrete crushing.

- For varied axial force ratios, failure mechanism of low confined column B is mainly governed by core concrete crushing in compression. Moreover, Column B shows severe capacity loss in comparison with column A. This is because, column B is low confined and suffers from severe inelastic buckling of vertical bars.
- Corrosion has a more significant impact on ductility loss of corroded RC columns than on flexural capacity. For example, 20% mass loss and 0.2 axial force ratio, results in 35% reduction in flexural capacity of column B, while for the same case the ductility loss is about 50%.
- The original HAZUS limit states cannot be used in fragility analysis of corroded structures. This is because corrosion reduces the ductility of the RC structures and also changes the failure mode. For example, in HAZUS the 0.08 drift ratio corresponds to complete collapse. However, in column B after 10% mass loss, the collapse load is at 0.05 drift ratio.
- The results of this study show that the damage limit states (mainly govern by ductility) that are for seismic fragility analysis of corroded structures, should be considered as time-variant parameters. The framework developed in this paper, provides a computational platform for other researchers to be used in seismic fragility analysis of corroded structures in future research.

References

Aligizaki, K. K. (1999). *Modeling of concrete cracking due to corrosion of embedded reinforcement*.

Alipour, A., Shafei, B., & Shinozuka, M. (2010). Performance evaluation of deteriorating highway bridges located in high seismic areas. *Journal of Bridge Engineering*.

American Society of Civil Engineers. (2013). Report Card for America's Infrastructure. http://www.infrastructurereportcard.org/a/#p/bridges.

Barrera, A., Bonet, J., Romero, M. L., & Fernández, M. (2012). Ductility of slender reinforced concrete columns under monotonic flexure and constant axial load. *Engineering Structures, 40*, 398-412.

Berry, M. P., & Eberhard, M. O. (2004). *Performance models for flexural damage in reinforced concrete columns*: Pacific Earthquake Engineering Research Center.

Berry, M. P., & Eberhard, M. O. (2005). Practical performance model for bar buckling. *Journal of Structural Engineering, 131*(7), 1060-1070.

Berry, M. P., & Eberhard, M. O. (2007). Performance modeling strategies for modern reinforced concrete bridge columns, Pacific Earthquake Engineering Research Center, University of California, Berkeley.

Berto, L., Vitaliani, R., Saetta, A., & Simioni, P. (2009). Seismic assessment of existing RC structures affected by degradation phenomena. *Structural Safety, 31*(4), 284-297.

Broomfield, J. P. (2002). *Corrosion of steel in concrete: understanding, investigation and repair*: CRC Press.

Camnasio, E. (2013). *Lifetime performance and seismic resilience of concrete structures exposed to corrosion.* Italy.

Chernin, L., & Val, D. V. (2011). Prediction of corrosion-induced cover cracking in reinforced concrete structures. *Construction and Building Materials, 25*(4), 1854-1869.

Chernin, L., Val, D. V., & Volokh, K. Y. (2010). Analytical modelling of concrete cover cracking caused by corrosion of reinforcement. *Materials and Structures, 43*(4), 543-556.

Chiu, C. K., Tu, F. J., & Hsiao, F. P. (2015). Lifetime seismic performance assessment for chloride-corroded reinforced concrete buildings. *Structure and Infrastructure Engineering, 11*(3), 345-362.

Choe, D.-E., Gardoni, P., Rosowsky, D., & Haukaas, T. (2008). Probabilistic capacity models and seismic fragility estimates for RC columns subject to corrosion. *Reliability Engineering & System Safety, 93*(3), 383-393.

Choine, M. N., O'Connor, A., & Padgett, J. E. (2013). *A seismic reliability assessment of reinforced concrete integral bridges subject to corrosion.* Paper presented at the Key Engineering Materials.

Coleman, J., & Spacone, E. (2001). Localization issues in force-based frame elements. *Journal of Structural Engineering, 127*(11), 1257-1265.

Coronelli, D., & Gambarova, P. (2004). Structural assessment of corroded reinforced concrete beams: modeling guidelines. *Journal of Structural Engineering, 130*(8), 1214-1224.

fib, F. I. (2006). Model code for service life design. *fib Bulletin, 34*.

Du, Y., Chan, A., & Clark, L. (2006). Finite element analysis of the effects of radial expansion of corroded reinforcement. *Computers & structures, 84*(13), 917-929.

Du, Y., Clark, L., & Chan, A. (2005a). Effect of corrosion on ductility of reinforcing bars. *Magazine of Concrete Research, 57*(7), 407-419.

Du, Y., Clark, L., & Chan, A. (2005b). Residual capacity of corroded reinforcing bars. *Magazine of Concrete Research, 57*(3), 135-147.

El Maaddawy, T., & Soudki, K. (2007). A model for prediction of time from corrosion initiation to corrosion cracking. *Cement and concrete composites, 29*(3), 168-175.

FEMA, F. (1999). Multi-hazard loss estimation methodology. *Earthquake model. HAZUS99 User's Manual. Washington (DC)*.

Fernandez I, Bairan JM, Mari AR (2015), "Corrosion effects on the mechanical properties of reinforcing steel bars. Fatigue and σ-ε behavior", Construction and Building Materials, 101, 772-783.

Fernandez I, Bairan JM, Mari AR (2016), "Mechanical model to evaluate steel reinforcement corrosion effects on σ-ε and fatigue curves. Experimental calibration and validation", Engineering Structures, 118, 320-333.

Ghosh, J., & Padgett, J. E. (2010). Aging considerations in the development of time-dependent seismic fragility curves. *Journal of Structural Engineering, 136*(12), 1497-1511.

Ghosh, J., & Sood, P. (2016). Consideration of Time-Evolving Capacity Distributions and Improved Degradation Models for Seismic Fragility Assessment of Aging Highway Bridges. *Reliability Engineering & System Safety*.

Guo, A., Li, H., Ba, X., Guan, X., & Li, H. (2015a). Experimental investigation on the cyclic performance of reinforced concrete piers with chloride-induced corrosion in marine environment. *Engineering Structures, 105*, 1-11.

Guo, A., Yuan, W., Lan, C., Guan, X., & Li, H. (2015b). Time-dependent seismic demand and fragility of deteriorating bridges for their residual service life. *Bulletin of Earthquake Engineering*, 1-21.

Jeon, J. S., Lowes, L. N., DesRoches, R., & Brilakis, I. (2015). Fragility curves for non-ductile reinforced concrete frames that exhibit different component response mechanisms. *Engineering Structures*, *85*, 127-143.

Kallias, A. N., & Rafiq, M. I. (2010). Finite element investigation of the structural response of corroded RC beams. *Engineering Structures*, *32*(9), 2984-2994.

Kashani, M. M., Lowes, L., Crewe, A., & Alexander, N.(2016a). Computational modelling strategies for nonlinear response prediction of corroded circular RC bridge piers. *Advances in Materials Science and Engineering*.

Kashani, M. M. (2014). *Seismic Performance of Corroded RC Bridge Piers*. University of Bristol.

Kashani, M. M., Alagheband, P., Khan, R., & Davis, S. (2015b). Impact of corrosion on low-cycle fatigue degradation of reinforcing bars with the effect of inelastic buckling. *International Journal of Fatigue, 77*, 174-185.

Kashani, M. M., Crewe, A. J., & Alexander, N. A. (2013a). Nonlinear cyclic response of corrosion-damaged reinforcing bars with the effect of buckling. *Construction and Building Materials, 41*, 388-400.

Kashani, M. M., Crewe, A. J., & Alexander, N. A. (2013b). Nonlinear stress–strain behaviour of corrosion-damaged reinforcing bars including inelastic buckling. *Engineering Structures, 48*, 417-429.

Kashani, M. M., Lowes, L. N., Crewe, A. J., & Alexander, N. A. (2014). Finite element investigation of the influence of corrosion pattern on inelastic buckling and cyclic response of corroded reinforcing bars. *Engineering Structures, 75*, 113-125.

Kashani, M. M., Lowes, L. N., Crewe, A. J., & Alexander, N. A. (2015a). Phenomenological hysteretic model for corroded reinforcing bars including inelastic buckling and low-cycle fatigue degradation. *Computers & Structures, 156*, 58-71.

Kashani, M. M., Lowes, L. N., Crewe, A. J., & Alexander, N. A. (2016b). Nonlinear fibre element modelling of RC bridge piers considering inelastic buckling of reinforcement. *Engineering Structures, 116*, 163-177.

Kowalsky, M. J. (2000). Deformation limit states for circular reinforced concrete bridge columns. *Journal of Structural Engineering, 126*(8), 869-878.

Li, X., Liang, Y.-S., Zhao, Z.-H., & Lv, H.-L. (2015). Low-cycle fatigue behavior of corroded and CFRP-wrapped reinforced concrete columns. *Construction and Building Materials, 101*, 902-917.

Liu, Y. (1996). Modeling the Time-to Corrosion Cracking of the Cover Concrete in Chloride Contaminated Reinforced Concrete Structures.

Liu, Y., & Weyers, R. E. (1998). Modeling the time-to-corrosion cracking in chloride contaminated reinforced concrete structures. *ACI Materials Journal, 95*(6).

Lowes, L.N., Altoontash, A., Mitra, N. (2005). Modeling Reinforced-Concrete Beam-Column Joints Subjected to Cyclic Loading. Journal of Structural Engineering,131(6), 993-994.

Lowes, L.N., Mitra, N., Altoontash, A. (2003). A beam-column joint model for simulating the earthquake response of reinforced concrete frames. Pacific Earthquake Engineering Research Center, College of Engineering, University of California.

Ma, Y., Che, Y., & Gong, J. (2012). Behavior of corrosion damaged circular reinforced concrete columns under cyclic loading. *Construction and Building Materials, 29*, 548-556.

Manson, S. (1965). Fatigue: a complex subject—some simple approximations. *Experimental mechanics, 5*(7), 193-226.

McKenna, F. (2011). OpenSees: a framework for earthquake engineering simulation. *Computing in Science & Engineering, 13*(4), 58-66.

Meda, A., Mostosi, S., Rinaldi, Z., & Riva, P. (2014). Experimental evaluation of the corrosion influence on the cyclic behaviour of RC columns. *Engineering Structures, 76*, 112-123.

Menegotto, M. (1973). *Method of analysis for cyclically loaded RC plane frames including changes in geometry and non-elastic behavior of elements under combined normal force and bending*. Paper presented at the Proc. of IABSE symposium on resistance and ultimate deformability of structures acted on by well defined repeated loads.

Ni Choine, M., Kashani, M. M., Lowes, L. N., O'Connor, A., Crewe, A. J., Alexander, N. A., et al. (2016). Nonlinear dynamic analysis and seismic fragility assessment of a corrosion damaged integral bridge. *International Journal of Structural Integrity, 7*(2), 227-239.

Ou, Y. C., Tsai, L. L., & Chen, H. H. (2012). Cyclic performance of large-scale corroded reinforced concrete beams. *Earthquake Engineering & Structural Dynamics, 41*(4), 593-604.

Poulsen, E., & Mejlbro, L. (2010). *Diffusion of chloride in concrete: theory and application*: CRC Press.

Priestley, M., & Paulay, T. (1992). Seismic design of reinforced concrete and masonry buildings. *New York: John Wiley & Sons, Inc*.

Pugh, J. S., Lowes, L. N., & Lehman, D. E. (2015). Nonlinear line-element modeling of flexural reinforced concrete walls. *Engineering Structures, 104*, 174-192.

Rao, A. S., Lepech, M. D., & Kiremidjian, A. (2016b). Development of time-dependent fragility functions for deteriorating reinforced concrete bridge piers 1. *Structure and Infrastructure Engineering*, 1-17.

Rao, A. S., Lepech, M. D., Kiremidjian, A. S., & Sun, X.-Y. (2016a). Simplified structural deterioration model for reinforced concrete bridge piers under cyclic loading 1. *Structure and Infrastructure Engineering*, 1-12.

Salami, M. R. (2017). Seismic Performance of Buildings Considering Mainshock-Aftershocks. University of Bristol.

Scott, B., Park, R., & Priestley, M. (1982). *Stress-strain behavior of concrete confined by overlapping hoops at low and high strain rates.* Paper presented at the ACI Journal Proceedings.

Shafei, B., Alipour, A., & Shinozuka, M. (2012). Prediction of corrosion initiation in reinforced concrete members subjected to environmental stressors: A finite-element framework. *Cement and Concrete Research, 42*(2), 365-376.

Tang, S., Yao, Y., Andrade, C., & Li, Z. (2015). Recent durability studies on concrete structure. *Cement and Concrete Research, 78*, 143-154.

Thoft-Christensen, P. (2005). *Service life definitions based on corrosion crack width.* Paper presented at the Proc., 9th Int. Conf. on Structural Safety and Reliability (ICOSSAR'05).

Titi, A. (2012). Lifetime probabilistic seismic assessment of multistory precast buildings.

Val, D. V. (2007). Factors affecting life-cycle cost analysis of RC structures in chloride contaminated environments. *Journal of infrastructure systems, 13*(2), 135-143.

Vamvatsikos, D., & Cornell, C. A. (2002). Incremental dynamic analysis. *Earthquake Engineering & Structural Dynamics, 31*(3), 491-514.

Vidal, T., Castel, A., & Francois, R. (2004). Analyzing crack width to predict corrosion in reinforced concrete. *Cement and Concrete Research, 34*(1), 165-174.

Vu, K. A. T., & Stewart, M. G. (2000). Structural reliability of concrete bridges including improved chloride-induced corrosion models. *Structural safety, 22*(4), 313-333.

Vu, N. S., Yu, B., & Li, B. (2016). Prediction of strength and drift capacity of corroded reinforced concrete columns. *Construction and Building Materials, 115*, 304-318.

Webster, M., & Clark, L. (2000). The structural effect of corrosion–an overview of the mechanism. *Proceedings of the Concrete Communication, Birmingham, UK*, 409-421.

Williamson, S., & Clark, L. (2000). Pressure required to cause cover cracking of concrete due to reinforcement corrosion. *Magazine of Concrete research, 52*(6), 455-467.

Yassin, M. H. M. (1994). *Nonlinear analysis of prestressed concrete sructures under monotonic and cyclic loads*: University of California, Berkeley.

Zhang, X., Wang, J., Zhao, Y., Tang, L., & Xing, F. (2015). Time-dependent probability assessment for chloride induced corrosion of RC structures using the third-moment method. *Construction and Building Materials, 76*, 232-244.